AD-A109 577 NAVAL POSTGRADUATE SCHOOL MONTEREY CA F/G 4/2
COMPARISON OF OVERWATER STABILITY CLASSIFICATION SCHEMES WITH M--ETC(U)
1982 G E SCHACHER, D E SPIEL, K L DAVIDSON
UNCLASSIFIED NPS-61-82-002 NL

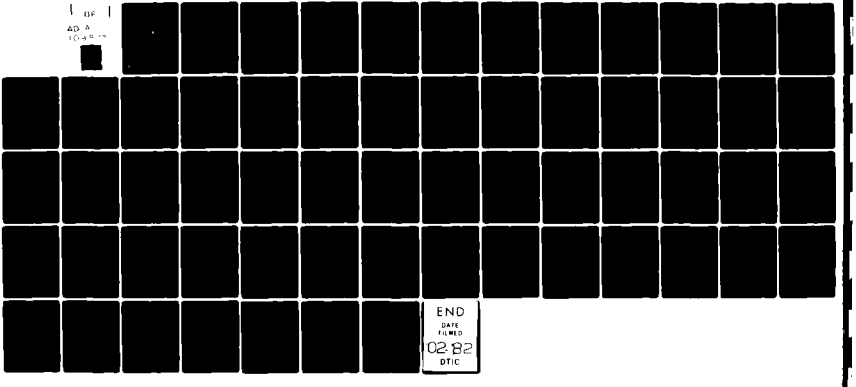

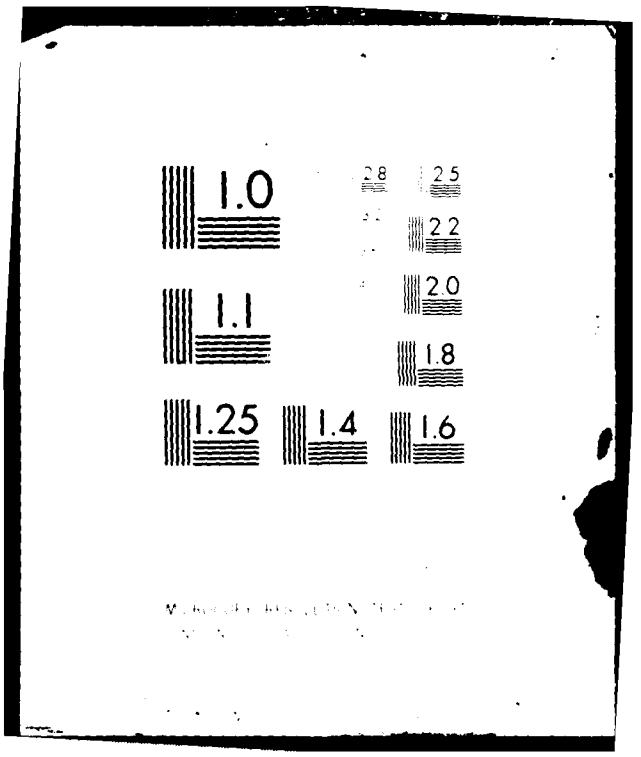
1.0
2.8
2.5
2.2
1.1
2.0
1.8
1.25
1.4
1.6

LEVEL

NPS-61-82-002

AD A109577

NAVAL POSTGRADUATE SCHOOL

Monterey, California

"Comparison of Overwater Stability Classification Schemes with Measured Wind Direction Variability"

G.E. Schacher, D.E. Speil
K.L. Davidson and C.W. Fairall
Environmental Physics Group
Naval Postgraduate School
Monterey, California

Approved for public release; distribution unlimited

Prepared for: Outer Continental Shelf Division
Bureau of Land Management
Los Angeles, California 90017

NAVAL POSTGRADUATE SCHOOL
Monterey, California

Rear Admiral J.J. Ekelund
Superintendent

David A. Schrady
Acting Provost

The work reported herein was supported with funds provided by the Outer Continental Shelf Division, Bureau of Land Management, Los Angeles, California 90017.

This report was prepared by:

G.E. SCHACHER
Professor of Physics

K.L. DAVIDSON
Associate Professor of Meteorology

Reviewed by:

J.N. DYER, Chairman
Department of Physics and Chemistry

Released by:

R.J. RENARD
Department of Meteorology

WILLIAM M. TOLLES
Dean of Research

UNCLASSIFIED

SECURITY CLASSIFICATION OF THIS PAGE (When Data Entered)

REPORT DOCUMENTATION PAGE		READ INSTRUCTIONS BEFORE COMPLETING FORM
1. REPORT NUMBER NPS 61-82-002	2. GOVT ACCESSION NO. AD-A109 377	3. RECIPIENT'S CATALOG NUMBER
4. TITLE (and Subtitle) "Comparison of Overwater Stability Classification Schemes with Measured Wind Direction Variability"		5. TYPE OF REPORT & PERIOD COVERED Technical Report 6. PERFORMING ORG. REPORT NUMBER
7. AUTHOR(s) G.E. Schacher, D.E. Spiel, K.L. Davidson C.W. Fairall		8. CONTRACT OR GRANT NUMBER(s) Interagency Agreement No. AA851-IAO-43
9. PERFORMING ORGANIZATION NAME AND ADDRESS Naval Postgraduate School Monterey, California 93940		10. PROGRAM ELEMENT, PROJECT, TASK AREA & WORK UNIT NUMBERS
11. CONTROLLING OFFICE NAME AND ADDRESS Outer Continental Shelf Division Bureau of Land Management Los Angeles, CA 90017		12. REPORT DATE 13. NUMBER OF PAGES 58
14. MONITORING AGENCY NAME & ADDRESS(if different from Controlling Office)		15. SECURITY CLASS. (of this report) Unclassified 15a. DECLASSIFICATION/DOWNGRADING SCHEDULE

16. DISTRIBUTION STATEMENT (of this Report)

Distribution unlimited

17. DISTRIBUTION STATEMENT (of the abstract entered in Block 20, if different from Report)

18. SUPPLEMENTARY NOTES

D.E. Spiel and C.W. Fairall are BDM contract employees.

19. KEY WORDS (Continue on reverse side if necessary and identify by block number)

20. ABSTRACT (Continue on reverse side if necessary and identify by block number)

Schemes for assessing atmospheric stability are described and a modification to the Pasquill scheme to parameterize it for the overwater regime is developed. The various schemes are compared to measured values of the wind direction standard deviation. The results are location specific, applying only to the California channel islands area.

DD FORM 1 JAN 73 1473 EDITION OF 1 NOV 65 IS OBSOLETE
S/N 0102-014-6601 |

UNCLASSIFIED

SECURITY CLASSIFICATION OF THIS PAGE (When Data Entered)

TABLE OF CONTENTS

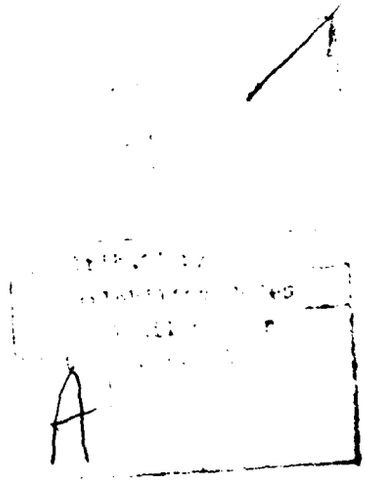

LIST OF TABLES

Figure Captions

1. Surface wind roses for Point Mugu as a function of month.

2. Average wind speed and direction as a function of time of day and time of year. The solid lines are wind speed isopleths (knots), the dashed lines indicate wind direction, where North is at the top of the figure, and land breeze and sea breeze regimes are approximately divided by the heavy broken line.

3. Pasquill classification boundaries as a function of the Monin-Obukhov stability length and the roughness length.

4. Dependence of 1/L on the wind speed and air-sea temperature difference for relative humidities of a) 50%, b) 80%, and c) 95%.

5. Pasquill classification boundaries as a function of wind speed and air-sea temperature difference.

6. Hourly average standard deviation of wind direction versus the air temperature difference between the 20m and 7m levels.

7. Hourly average standard deviation of wind direction versus the air-sea temperature difference.

8. Hourly average standard deviation of wind direction versus the reciprocal of the Monin-Obukhov length.

9. Wind direction variance versus the ln of the stability parameter. The open circles are averages for the bins $-10/L < 0.1$, $0.1 \leq -10/L < 0.2$, $0.2 \leq -10/L < 0.5$, $0.5 \leq -10/L < 1.0$, $1.0 \leq -10/L$. The solid line is the linear regression to the data.

10. Wind direction variance as a function of wind direction and the stability parameter.

11. Wind direction variance for the overwater Pasquill classes. The shaded regions show the recommended class-variance groups.

I. Introduction

During September of 1980 and January of 1981 the Naval Postgraduate School (NPS) and Aerovironment, Inc. (AI) conducted an intensive series of tracer measurements off Ventura, California in the Santa Barbara Channel. The main purpose of these experiments was to parameterize Gaussian and trajectory dispersion models for the overwater regime. A secondary purpose was to build a data base for future model development.

The experimental procedure was as follows: SF_6 gas was released from the NPS research ship RV/Acania at a rate of approximately 50 lbs/hr. The ship was anchored at a point approximately 5 miles from shore. The position and dimensions of the plume were determined at three downwind distances by analyzers aboard an aircraft and van, and by collecting gas samples at fixed shore locations and from a small boat. The plume analysis and shore based meteorological measurements were performed by AI. A complete characterization of the overwater meteorology, including stability, surface fluxes, and horizontal wind direction variance was obtained by NPS.

Data volumes for both experiments[1] and a final report on the results of the analyses will be available. The purpose of this report is twofold: to present the wind direction variance results, which are not included in the former data reports, and to present results comparing measures of overwater stability and the wind variance. In order to describe the conditions for which the data were obtained, a brief section describing the locality and observed meteorological conditions is included.

II. Meteorological Conditions during the Experiment

The area near Ventura, where the tracer experiments were performed, is representative of the general channel islands region but not of the majority of the California coastal region. It is an area where the weather is controlled by the interplay of numerous local influences* and the mesoscale features which are typical of the rest of the coast. The area lies within the embayment formed by the Santa Barbara Channel, Santa Monica Bay, and the Gulf of Santa Catalina. The Oxnard plane is approximately 20 miles long, extends from the beach to five to ten miles inland and is surrounded by coastal hills with peaks two to three thousand feet high. Within 40 miles inland mountains extend to 8,000 feet.

The geographic features cause many effects, the major ones being:

1. The mountains to the North act as a partial barrier to air mass movement from the North.
2. The mountains and the general east-west orientation of the shore produce a complex pattern of eddies.
3. Surrounding high hills contain the cool moist marine air. Only infrequent, strong, synoptic air mass changes displace the marine air.
4. The surrounding hills and mountain valleys channel the air flow into complex patterns.

* Much of the description of the local meteorology presented here is exerpted from Pacific Missile Test Center documents, which are listed in the reference section as reference 2.

5. Heating of local slopes "draws in" the afternoon sea breeze, and nightime cooling and the resulting drainage reverses the local flow. The diurnal cycle is very persistant.
6. During periods of storms with strong southerlies, the common rain pattern, the wind is turned to southeasterly and accelerated.

Because of the complexity of the local influences any measurements made in this area are not representative of the open coast but are location specific.

It is difficult to obtain sufficient data in a given area to parameterize a model for all conditions that may be encountered. This experiment was conducted for two approximately two-week periods, one in the late summer and one in the winter. With a limited data set one must compare the meteorological conditions encountered with typical conditions for the locality then attempt to extend the results to other conditions that are frequently encountered. Extreme conditions cannot normally be treated. For comparison purposes, we list below the normal seasonal conditions in the Ventura area and conditions encountered during the experiments. This will constitute the meteorological framework for discussing the tracer experimental results.

A. Seasonal Conditions in the Ventura Area

Summer

The North Pacific Semipermanent Subtropical High lies to the west of the area and controls the synoptic scale. Clockwise flow around the high produces northwesterlies along much of the coast; this flow is turned more westerly by the Point Conception/mountain geographic influence. The local sea breeze turns the wind further to a westerly or southwesterly. The general onshore flow is aided by the inland thermal trough which is created by overland heating. Strong subsidence creates the prevalent capping inversion. The occasional passage of weak upper level troughes will dissipate or lift the inversion for short periods of time.

Fall

The building of high pressure in the Great Basin causes frequent Santa Ana conditions. The pattern of storms and upper level westerlies moves further south breaking up the summer pattern. Frontal passage becomes more frequent and the subtropical high becomes displaced or shrinks, resulting in a break up of the marine inversion.

Winter

Frontal passage becomes much more frequent and strong surface westerlies often follow the passage. Santa Ana winds can still occur when the surface pressure in the Great Basin becomes sufficiently high. Also, the Pacific High and capping inversion can reform between frontal passage occurrences.

Spring

As the storm pattern moves north, the Pacific High again becomes the dominant feature. Cold lows pass frequently, followed by strong westerlies.

B. Wind Climatology

Although the strong local influences make it difficult to accurately predict the wind in the Ventura area, the seasonal patterns are quite reproducable. This makes a climatology useful for assessing expected onshore impact. Only a wind climatology is presented here since that is our primary concern.

Surface wind roses for each month are shown in Figure 1. Wind speed is indicated by the width of each "vector", wind direction by the angle, and frequency of occurrence by the length. The numbers in each wind rose circle are the percent of the time the wind is $\leq$4 knots.

Average prevalent wind as a function of time of day and time of year are shown in Figure 2. The dashed lines show wind direction, where a vector from top to bottom on the page indicates a north wind. The solid lines are wind speed isopleths. The heavy dashed lines approximately divide the land and sea breeze regimes.

Of special interest are the frequency of strong winds, the frequency of occurrence of Santa Anas, and the most frequently observed direction. This information is given in Table [1].

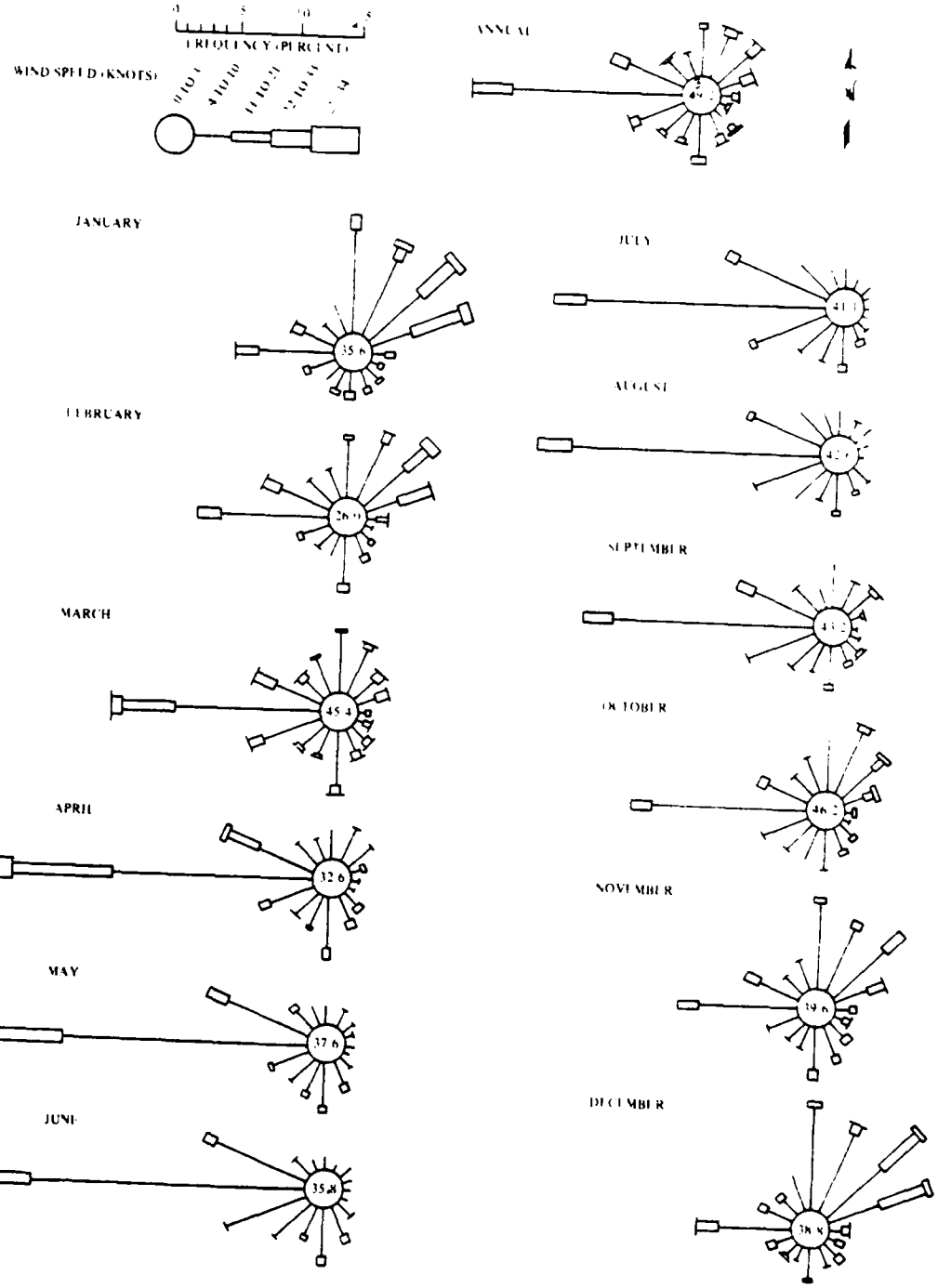
FREQUENCY (PERCENT)
WIND SPEED (KNOTS)
ANNUAL
JANUARY
JULY
FEBRUARY
AUGUST
SEPTEMBER
MARCH
OCTOBER
APRIL
NOVEMBER
MAY
DECEMBER
JUNE

Figure 1

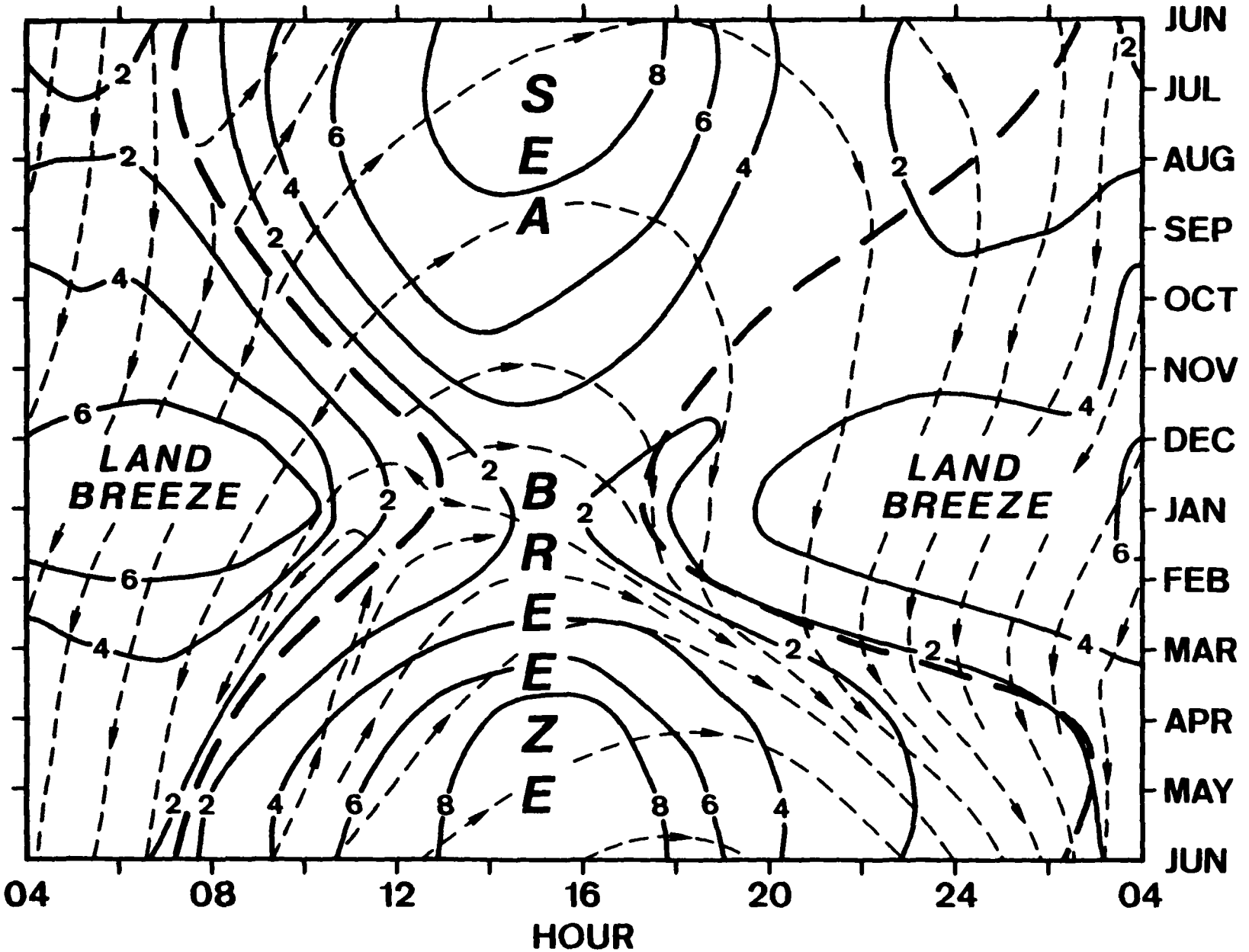
SEA
BREEZE
LAND BREEZE
LAND BREEZE
JUN
JUL
AUG
SEP
OCT
NOV
DEC
JAN
FEB
MAR
APR
MAY
JUN
04
08
12
16
20
24
04
HOUR

Figure 2

C. Weather Description for the Test Periods

The following information is derived from the daily weather maps, weekly series, published by the National Oceanic and Atmospheric Administration. The periods of interest are 9/24-9/29, 1980 and 1/6-1/15, 1981. For completeness we describe the situations for periods slightly longer than the duration of the experiments.

9/24-9/29: Throughout the period a strong thermal low persisted in northwestern Mexico.

9/22: Surface highs were centered over the Northwest and Wyoming and pressure gradients in the western US were weak. Strong onshore flow was not expected.

9/23: Surface highs were located over Colorado. Pressure gradients were even weaker.

9/24: Surface highs were moving in off Canadian coast. A weak upper level ridge was forming in the same area and a weak trough forming over north central US. Surface gradients were increasing off the California coast causing weak onshore flow.

9/25: Surface highs were located over the northern portion of the continent. The upper level ridge was strengthening but only over the area north of California. The trough over central US was strengthening. Only very weak surface gradients existed in the coastal region.

9/26: Surface low was on the Washington coast and very large high covering the Midwest. The upper level ridge over western Canada was strong but did not extend south to California; the trough was moving to the East coast. The gradients were somewhat

higher, weak onshore flow was expected.

9/27: The situation was much the same as on 9/26 with additional highs over the northern US and a weak front moving in off Washington.

9/28: The pattern continued with the addition of a weak frontal passage north of San Francisco and some trailing precipitation.

9/29: A large surface high was centered over Idaho and Nevada. The upper level North-South ridge moved east to extend from Canada into Montana. Location of the high caused weak Santa Ana conditions.

9/30: The thermal low over nothwestern Mexico weakened, essentially disappearing. The whole of western US was dominated by surface high pressure.

General Comments: The whole period was dominated by the Pacific high. All frontal activity was to the north of California. The thermal low over Mexico was not strong enough to produce a dominant onshore flow, the surface pressure gradients in the coastal region being very weak. The local flow was dominated by the diurnal land-sea breeze cycle. Low subsidence inversions were present under the dominant high pressure. Weak Santa Ana conditions can occur under these conditions.

1/6-1/15: We do not give a day by day description as for the previous period. The two periods were similar and general comments will suffice to describe the situation. The Pacific high was unusually strong producing a mini-drought for what is normally

the beginning of the rainy season for California. Frontal passages were again far to the north. There was no well established onshore flow regime except for a short period during 1/12-1/13 when the surface gradient in the Southern California area increased. As before, the land-sea breeze cycle would dominate, however, fairly persistent highs over the inland western US strengthened the offshore flow so that periods of sea breeze were shortened.

	Most Frequent Wind				Santa Ana Occurrance	
Month	Direction	Speed	%	% greater than 21 knots	Average No. days	Maximum No. days
JAN	NE	10	15.5	2.3	9.3	16
FEB	W	9	12.3	1.8	5.2	12
MAR	W	10	18.3	1.1	2.8	8
APR	W	10	26.7	1.4	0.6	2
MAY	W	9	28.7	0.3	0.3	2
JUN	W	8	27.5	0.0	0	1
JUL	W	7	25.2	0.0	0	0
AUG	W	8	23.6	0.0	0	0
SEP	W	7	19.5	0.1	0.4	4
OCT	W	7	16.3	0.5	2.7	8
NOV	NE	7	12.1	1.0	7.0	19
DEC	N	5	12.8	1.4	9.3	18

Table 1. Monthly averages of the most frequently observed wind direction, percent of time the wind speed is greater than 21 knots, and the number of days of Santa Ana winds per month. The maximum number is the maximum observed over a ten year period.

III. Wind Direction Variance

The wind direction was measured by a vane mounted on the RV/Acania 20m above the water line. The vane responded to both the wind and to ship roll; since the ship normally pointed into the wind during the measurements, pitch had little effect. Ship direction, measured by a gyrocompass, and ship roll were determined and logged by a computer approximately every 1.5 sec. A pendulum mounted on the roll axis of the ship was used to measure roll. The roll induced transverse component of wind at the vane is the roll rate times the distance from the roll axis to the vane.

The wind data were processed and stored in two ways. Mean wind direction and speed were determined for half-hour periods. A correction for the ship direction was applied to the wind data when determining this average. A roll correction was not made since the short period roll, approximately 10-sec, averages to zero over a half-hour period. Wind direction was also averaged for 10-sec periods and these averages stored for later processing to determine the variance. The wind data was corrected for the ship roll component and ship heading for each 1.5-sec wind determination.

Hourly averages of wind direction and standard deviations are presented in Table 1. Note that the averages are not exactly one hour since they are compiled from the half-hour data acquisition periods and there is dead time for processing and printing at the end of each acquisition period.

Table 2. Hourly averages of wind directions and their standard deviations.

Data/Time	Average Direction	Sigma
9/24		
1109-1205	231	13.3
1206-1301	231	12.9
1303-1357	252	11.5
1358-1453	262	7.7
1455-1549	254	8.0
1551-1645	262	7.1
1743-1837	275	6.0
9/27		
0647-0743	43	6.3
0917-1013	279	10.2
1110-1206	270	6.6
1207-1302	274	5.6
1303-1358	273	4.7
1359-1454	272	4.0
1456-1550	275	2.4
1551-1646	273	2.9
1647-1742	268	2.8
1774-1838	269	3.6
9/28		
1239-1335	231	10.3
1340-1436	247	7.8
1437-1532	257	7.4
1534-1628	253	4.9
1712-1808	260	4.4
1809-1904	257	4.5
9/29		
1149-1245	229	5.1
1251-1347	253	5.0
1349-1443	262	3.3
1444-1540	261	3.9
1558-1654	266	2.4
1656-1750	268	5.2
1751-1846	285	3.8
1/6		
1125-1225	289	13.7
1325-1425	297	11.6
1425-1542	292	22.6
1542-1642	301	13.3
1642-1742	279	9.5
1742-1842	281	17.1
1842-1942	342	50.7
1/9		
1119-1221	278	10.6
1239-1339	273	6.7
1339-1439	281	3.4
1440-1539	279	4.8
1540-1639	276	9.2
1640-1739	272	3.1
1/13		
0822-0948	11	21.1
1019-1119	299	11.2
1209-1309	298	5.6
1310-1409	287	5.9
1409-1509	271	11.8
1509-1559	255	7.4
1559-1659	240	8.6
1/14		
1100-1200	181	46.5
1200-1300	213	23.6
1300-1400	194	15.6
1400-1500	246	22.6
1/15		
1411-1500	204	17.3
1522-1622	282	32.7
1622-1722	289	6.5
1/16		
0908-1008	344	12.7
1020-1120	324	5.6
1120-1220	336	6.2
1220-1320	335	8.9
1320-1420	319	17.7
1420-1520	298	4.6
1520-1620	295	4.3
1621-1720	295	4.8
1721-1820	294	8.0
1821-1920	299	6.8
1921-2020	271	53.2
2021-2120	195	44.3
2121-2220	277	8.8

IV. Stability Classification

It is common to use some measure of the stability of the atmosphere to determine the expected dispersion of a plume. The relationship between the three dimensional spreading and stability is complex and will not be discussed here. We present the various classification schemes and their interrelations. Since the Pasquill classification is so widely used we will show the method we use to modify it for the overwater regime. Our normal method for determining stability is to calculate the Monin-Obukhov length. In what follows we will compare the measured wind direction variance to this length and to the modified Pasquill classes to assess the usefulness of the classification schemes.

Atmospheric stability depends on the heat flux, which is a result of the temperature gradient, and the amount of mechanical turbulence which is generated by the wind. Several schemes for specifying the stability are in current use; all require a measurement or an estimate of the flux and turbulence. The methods we briefly describe here are the Monin-Obukhov length, the Richardson number, the Pasquill classifications, and an EPA method for relating the Pasquill class to the temperature gradient.

A. Monin-Obukhov Length

The Monin-Obukhov length can be determined from measured gradients of wind, temperature, and water vapor content in the surface layer. Gradients are difficult to measure, especially from a moving platform such as a ship. Under such conditions

it is preferable to use the bulk aerodynamic method, the measurements required being sea-surface temperature and wind speed, temperature, and water vapor content at a reference height. One assumes that the wind speed is zero and that the relative humidity is 100% at the surface. The air-surface differences in these bulk parameters are used to calculate surface layer fluxes and stability. The measurements must be made in the "surface layer", which is a layer approximately 30m thick, where the heat flux and friction velocity can be assumed constant.

The Monin-Obukhov length is calculated from

$$L = (T/kg)(U_*^3/Q), \tag{1}$$

where T is the absolute temperature, k is Von Karman's constant (0.35), g the acceleration due to gravity, and U_* the friction velocity (scaling velocity). The temperature flux, Q, is related to the virtual heat flux, H, by

$$H = \rho C_p Q, \tag{2}$$

where ρ is the air density and C_p is the specific heat at constant pressure. Note that for upward heat flux (unstable air) L is negative and is positive for downward heat flux (stable air). We will work with 1/L in what follows, which has the value zero for neutral conditions where the heat flux is zero. The temperature flux is directly related to the virtual potential temperature scaling parameter, Θ_{V*}, by

$$\begin{aligned} Q &= U_* \Theta_{V*} \\ &= U_*(\Theta_* + 6.1 \times 10^{-4} Tq_*), \end{aligned} \tag{3}$$

where q_* is the water vapor mixing ratio scaling parameter (gm/kg). The potential temperature is $\Theta = T + 0.0098Z$. We see that L can be calculated from the surface layer fluxes, or the scaling parameters, since they are directly related.

Briefly, the method we use is to determine the scaling parameters directly from the measured mean values using stability corrected drag coefficients. Note that this leads immediately to an iterative calculation since the stability must be known to determine the proper drag coefficient, stability (L) is determined from the scaling parameters, and the scaling parameters depend on the drag coefficient. The procedure is fairly simple and is described in detail in Appendix A.

B. Richardson's Number

We do not use the Richardson's number in what follows, but since it is often used, we present it here for the sake of completeness. Like the Monin-Obukhov length it can be determined from either bulk or gradient measurements. The gradient Richardson's number, determined from a two level measurement is

$$Ri = Z(g/T)[(\Theta_2 - \Theta_1)^2/(U_2 - U_1)]\ln(Z_2/Z_1), \qquad (4)$$

where the subscripts 1 and 2 refer to specific heights and Z is the geometric mean height. The bulk Richardson's number is determined from

$$B = Z(g/T)(\Theta - \Theta_o)/U^2, \qquad (5)$$

where Θ_o is the surface value. Ri and L can be approximately related to each other by

$$1/L = Ri/Z \quad \text{(unstable)} \tag{6}$$

and

$$1/L = Ri/Z(1 - \beta Ri) \quad \text{(stable)} \tag{7}$$

The value of β is taken to be 7, although this parameter is not well known.

C. Pasquill Class

The Pasquill classification is a simplified scheme which requires a determination of wind speed but not temperature. A heat flux category is determined from an estimation of the solar insolation at the surface. The scheme has been developed for overland use and is not appropriate for the overwater regime because of the vastly different thermal properties of water. Stability is divided into five classes, A-F, determined as follows:

	Daytime Insolation			Nightime Cloud Cover	
U(m/sec)	Strong	Moderate	Small	>4/8	<3/8
<2	A	A-B	B		
2	A-B	B	C	E	F
4	B	B-C	C	D	E
6	C	C-D	D	D	D
>6	C	D	D	D	D

In this scheme A-C are unstable, D neutral, and E-F stable conditions. This classification scheme is imprecise but, due to its simplicity, is in widespread use. One of our purposes here is to deduce a similar scheme for use in the overwater regime, and which will be more precise than the Pasquill categories.

D. EPA Temperature Gradient Classification

The Environmental Protection Agency has guidelines[3] for relating the Pasquill classifications to the wind direction standard deviation, σ_θ, and also to the temperature gradient in the surface layer. This scheme considers only the temperature gradient; no determination of the wind is used. Categorization is as follows:

$\Delta T/\Delta z$ (°C/100m)	Pasquill Class	σ_θ (deg)
<-1.9	A	≥22.5
-1.9 → -1.7	B	22.5 → 17.5
-1.7 → -1.5	C	17.5 → 12.5
-1.5 → -0.5	D	12.5 → 7.5
-0.5 → 1.5	E	7.5 → 3.8
1.5 → 4.0	F	<3.8
>4.0	G	

It is important to realize that this scheme was also developed by examination of overland data; it is not expected to be valid over water.

V. Modification of Pasquill Classification for Overwater Use

As has been stated above, the Pasquill classification scheme was derived for overland use. The overwater regime is different because of the vastly different response of water to incoming solar radiation and the variation of roughness length with wind speed. Because of the widespread use of this scheme we here modify it for overwater use; this should not be interpreted as a recommendation that this scheme remain in common use.

Golder[4] has related the Pasquill class boundaries to the roughness length and the Monin-Obukhov length. The results are shown in Figure 3. The dependence of the roughness length on wind speed has received much attention. We have chosen the parameterization of Kondo[5], which is detailed in Appendix A. Figure 3 has both wind speed and roughness length scales; the wind speed scale was derived from this parameterization.

Wind speed, temperature, and relative humidity (or dew point) are the meteorological parameters which are commonly measured, not 1/L. Of course, 1/L can be determined from the mean parameters by the method described in Appendix A. We have calculated 1/L as a function of wind speed, air-sea temperature difference (T_A-T_S), and relative humidities of 50%, 80%, and 95%. The results are shown in Figures 4. Also plotted on these figures are the boundaries of the Pasquill classes, as determined from Figure 3. Note that classes A and F do not appear on Figures 4 because these classes are outside the range of parameters that can be expected to occur over water (particularly, very large air-sea temperature difference).

Finally, using Figures 4, we plot the Pasquill class boundaries as functions of wind speed and T_A-T_S in Figure 5.

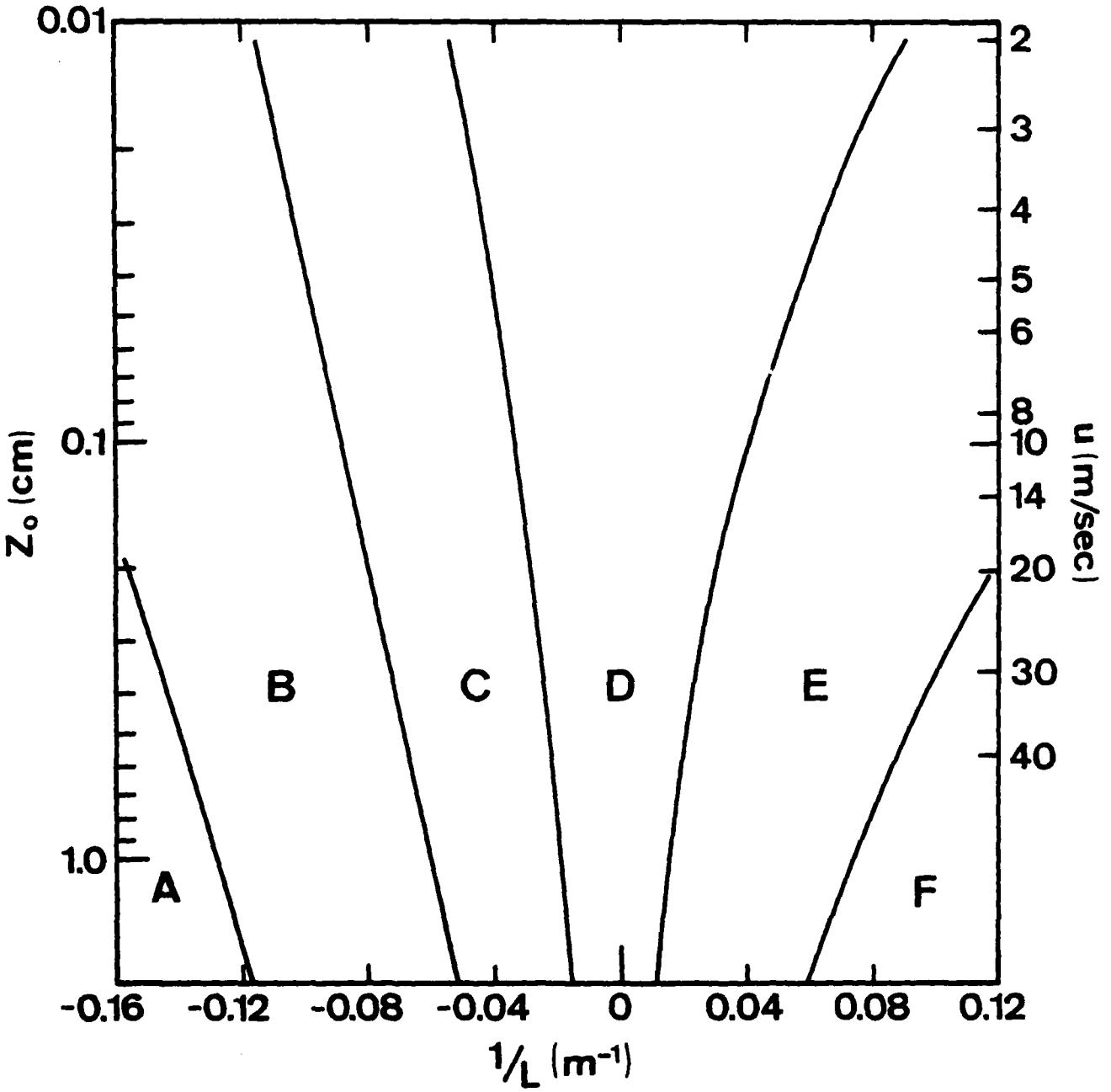
0.01
0.1
1.0
Z_o (cm)
2
3
4
5
6
8
10
14
20
30
40
u (m/sec)
A
B
C
D
E
F
-0.16
-0.12
-0.08
-0.04
0
0.04
0.08
0.12
$1/L$ (m^{-1})

Figure 3

There are three plots, one each for 50%, 80%, and 95% relative humidity. The humidity is not a major factor; it is most important near neutral (small T_A-T_S) where high humidity shifts the curves toward greater instability.

Note that all of the above calculations have been made for a height of 20m, for the measured mean parameters.

Because of the wide range of parameters applicable for each class, particularly D, we have arbitrarily divided each class into three subclasses, each subclass representing one third of the original class. For example, D+, D, and D- where the +/- refer to the stable/unstable side of the original class.

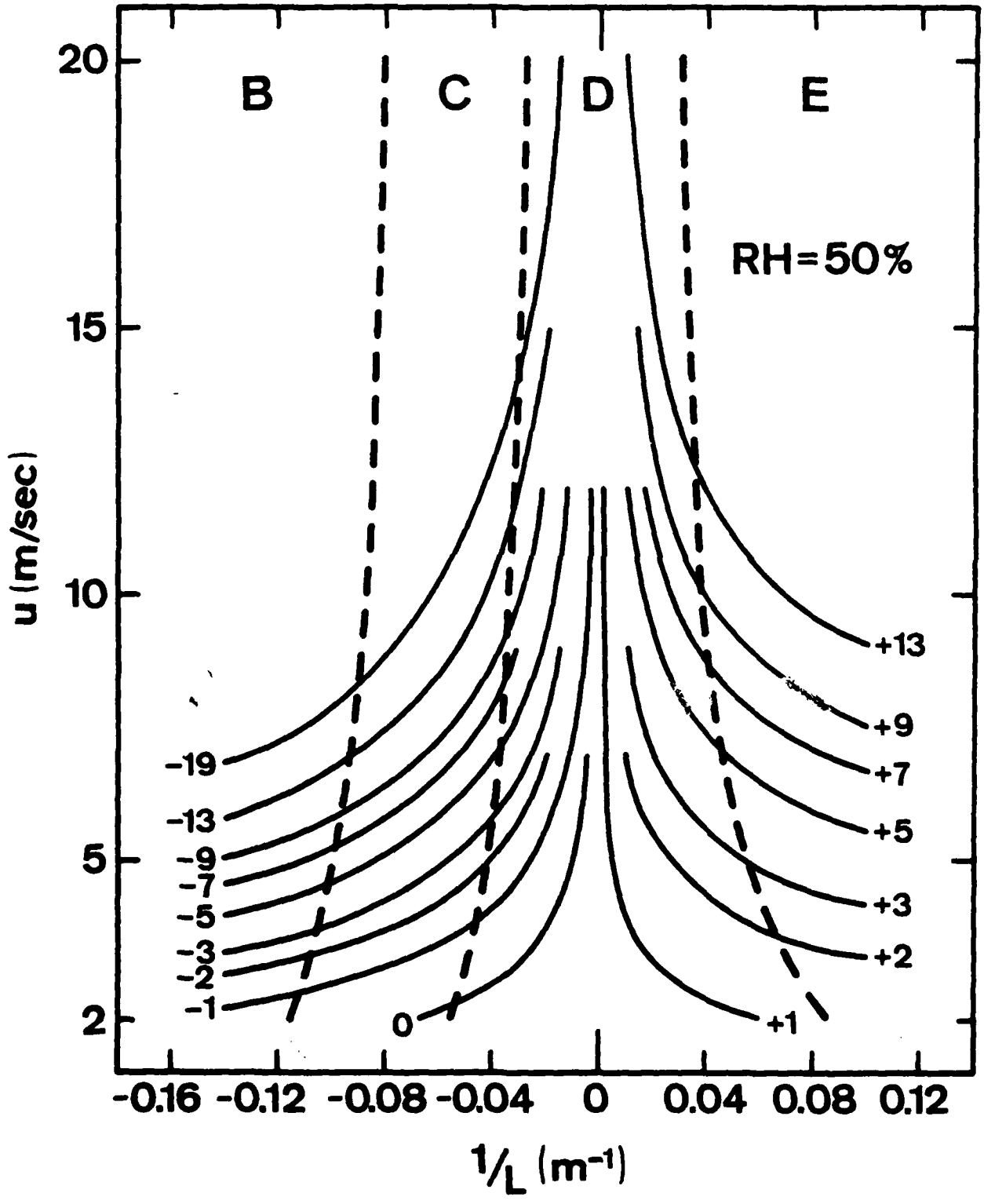
B
C
D
E
RH=50%
20
15
10
5
2
u (m/sec)
-19
-13
-9
-7
-5
-3
-2
-1
0
+1
+2
+3
+5
+7
+9
+13
-0.16
-0.12
-0.08
-0.04
0
0.04
0.08
0.12
1/L (m-1)

Figure 4a

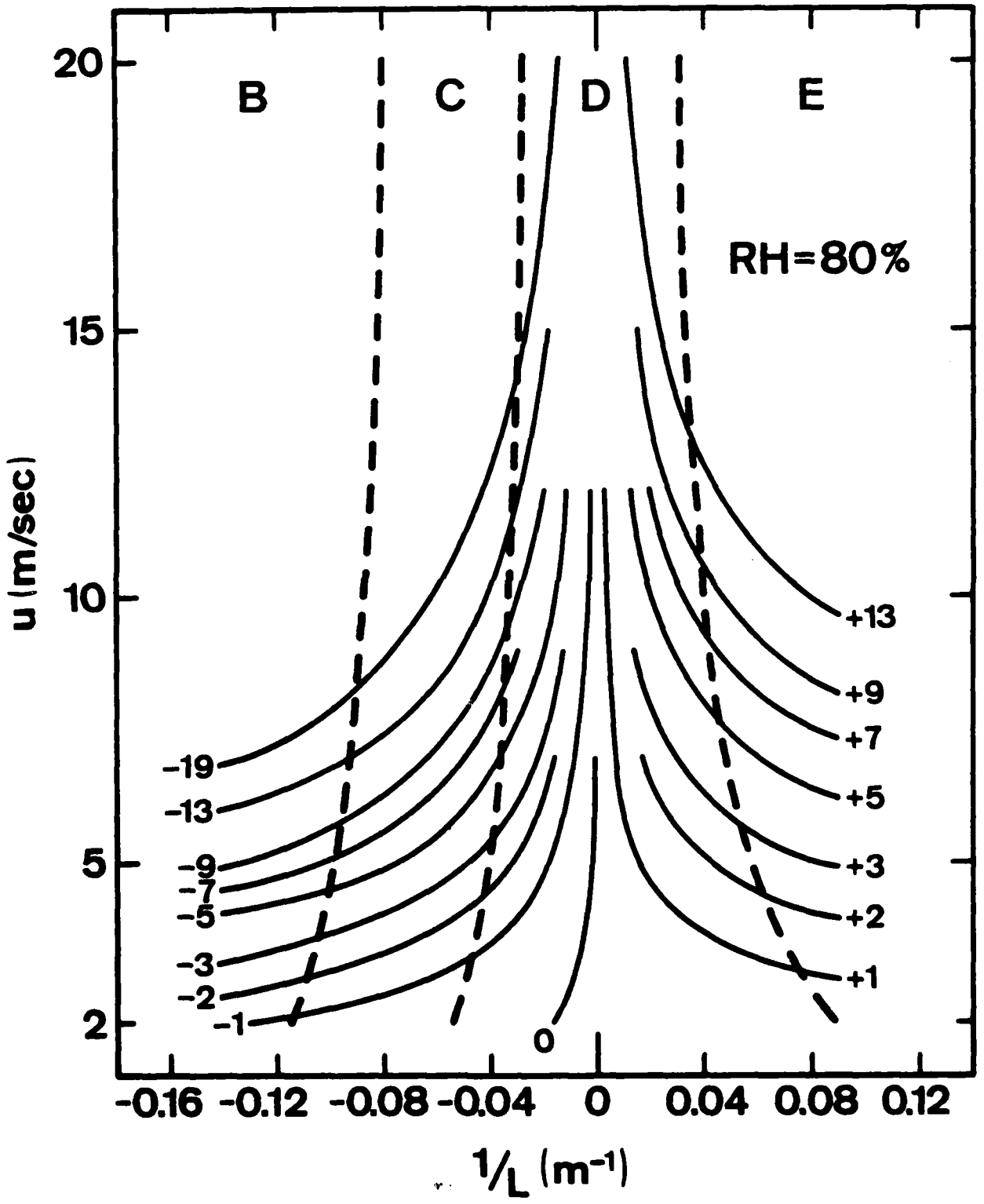
B
C
D
E
RH=80%
20
15
10
5
2
u (m/sec)
-19
-13
-9
-7
-5
-3
-2
-1
0
+13
+9
+7
+5
+3
+2
+1
-0.16 -0.12 -0.08 -0.04 0 0.04 0.08 0.12
1/L (m⁻¹)

Figure 4b

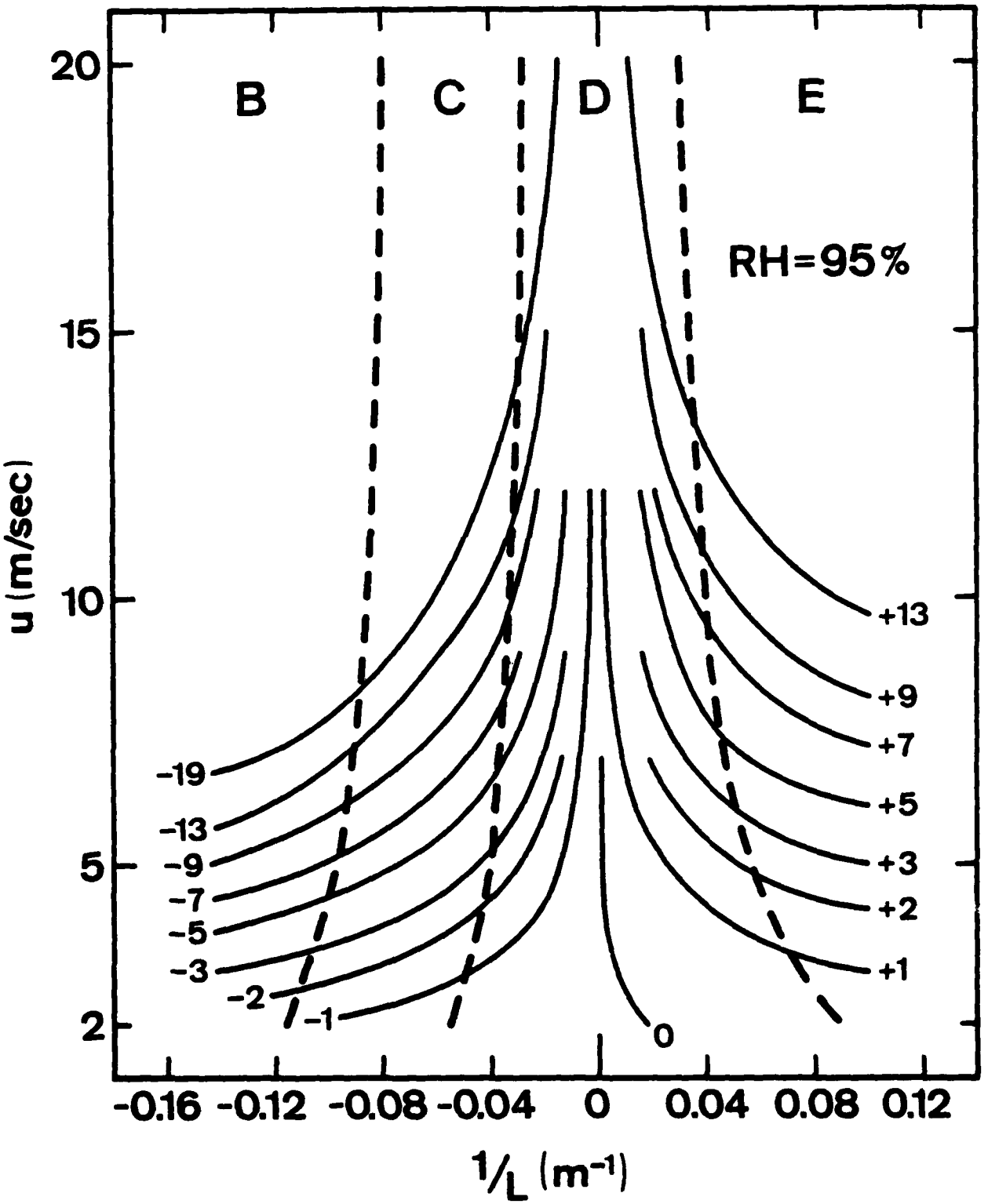
B
C
D
E
RH=95%
20
15
10
5
2
u (m/sec)
-19
-13
-9
-7
-5
-3
-2
-1
0
+13
+9
+7
+5
+3
+2
+1
-0.16 -0.12 -0.08 -0.04 0 0.04 0.08 0.12
1/L (m⁻¹)

Figure 4c

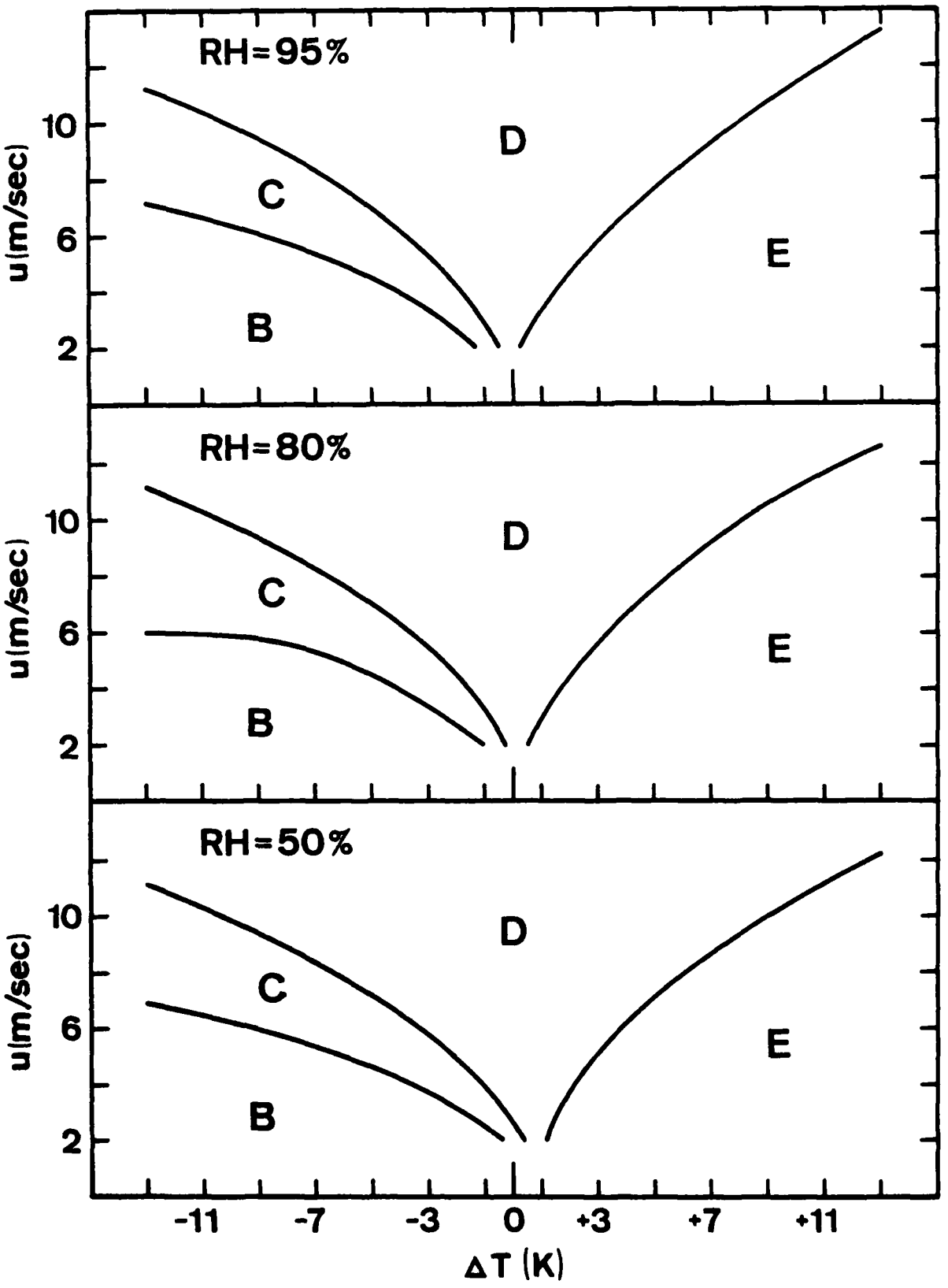

Figure 5

VI. Comparison of Classification Schemes with σ_θ

The ultimate test of any classification scheme is how well it can predict the behavior of a plume. Such a comparison for the data set gathered in this experiment is being made by AI. An equivalent test can be made by comparing to the variability of the wind direction, which, of course, is the major cause of cross wind spreading of a plume. This is the approach taken here. Short term (high frequency) fluctuations will cause spreading of a plume about its center line while long term variations will cause plume meander. One-hour average measurements of the plume concentration profile and one-hour averages of the wind direction standard deviation will both include short and long term variability. In this report, we will make only comparisons for long term averages since the purpose here is to parameterize models that compute one-hour average impact. The data set used (shown in section III) includes periods when tracer gas was not released. Measured values of σ_θ at a single point can be used to calculate the plume profile only if horizontal homogeneity exists.

We have compared the measured values of σ_θ with

A. air-sea temperature difference and temperature gradient

B. 10/L

C. modified Pasquill class

The air-sea temperature difference and temperature gradient are examined because of the EPA quidelines. We do not expect them to be of much use because stability cannot be determined from temperature information alone.

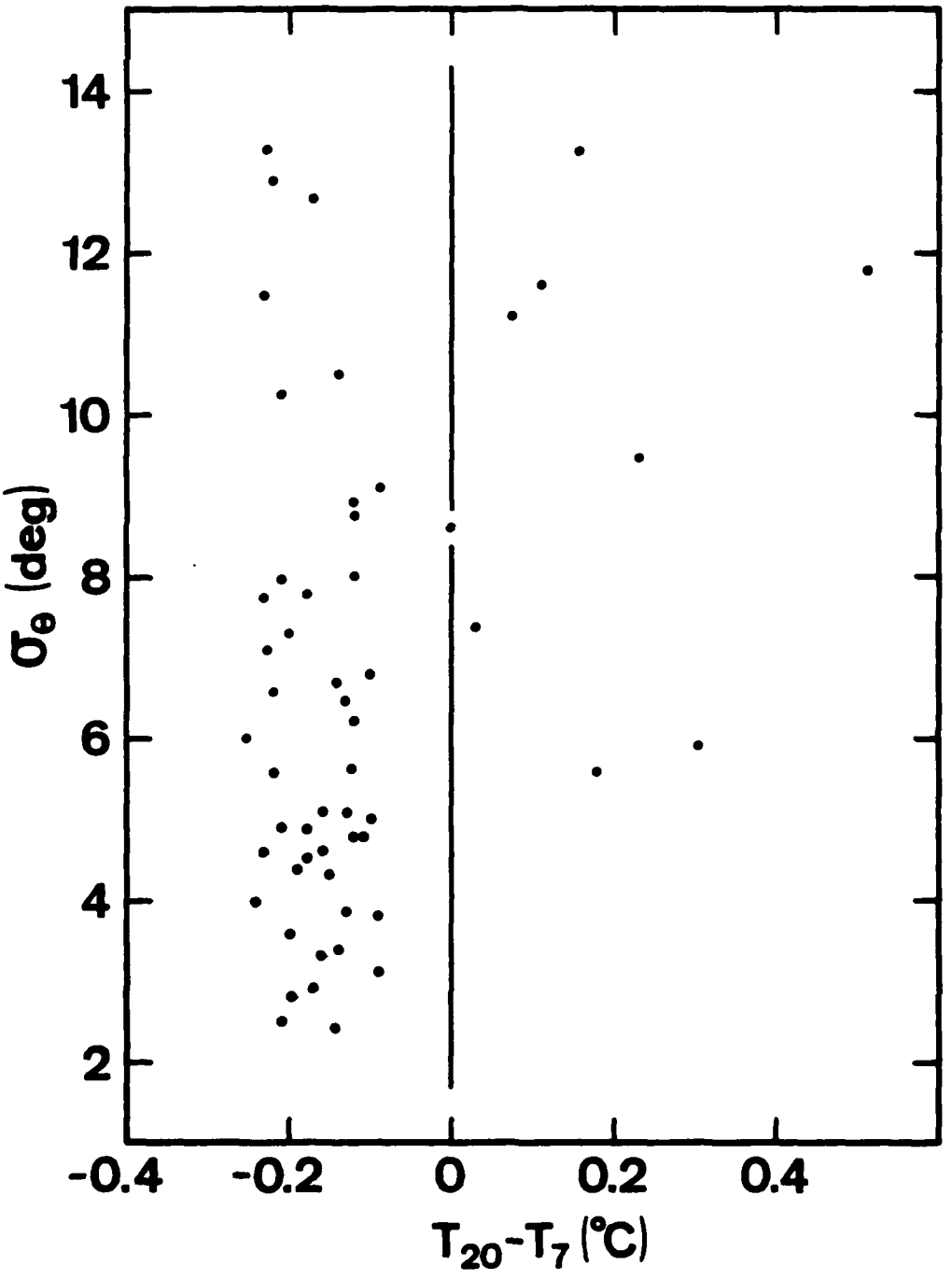

Figure 6

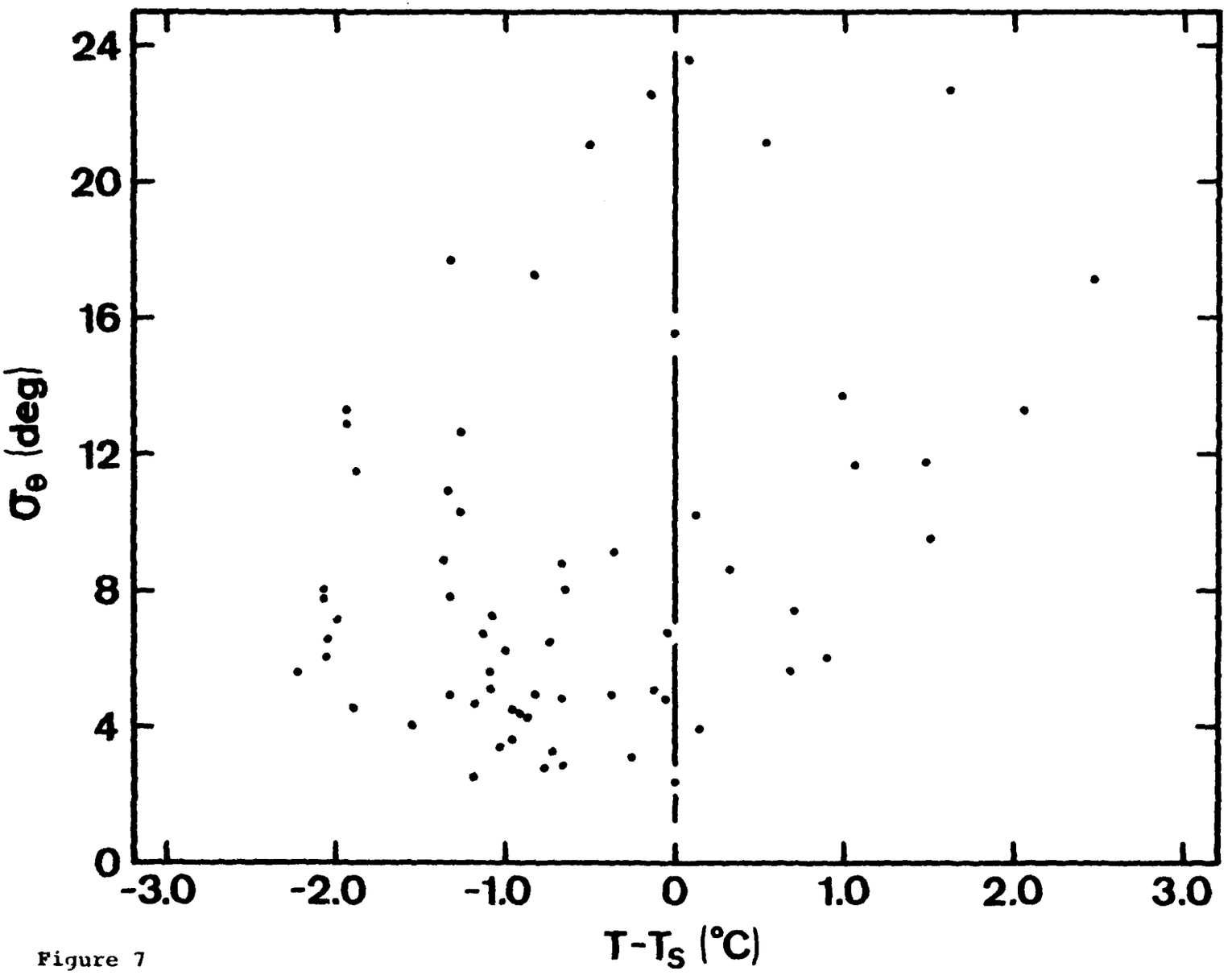

Figure 7

A. Air-Sea Temperature Difference and Temperature Gradient

On the ship the air temperature at 7m and 20m above sea level, and the sea surface temperature, T_S, were measured continuously and averaged every half hour. A description of the measurements and equipment used is given in Appendix B. For air-sea temperature difference we used $(T_{20}-T_S)$ and for temperature gradient we used $(T_{20}-T_7)$ directly, not dividing by the height difference. σ_θ versus $(T_{20}-T_7)$ and $(T_{20}-T_S)$ are shown in Figures 6 and 7, respectively.

There is little correlation between σ_θ and these parameters so, as expected, it would be very difficult to determine σ_θ from temperature measurements alone. For the sake of completeness we did a linear regression for both sets of data for negative temperature gradient. There is not enough data for negative temperature gradient. There is not enough data to warrant the calculation for positive gradient. The correlation coefficients of the linear regressions were only 0.14 for the gradient and 0.18 for the air-sea difference. It is interesting to note that $(T_{20}-T_S)$ values range from -2 to +2 C° whereas the range of $(T_{20}-T_7)$ is a factor of ten smaller. This emphasizes the difficulty in measuring temperature differences in the air over the ocean. The differences are normally too small to yield reliable results. It is much better to use the air-sea temperature difference when stability is being determined.

B. $10/L$

We have compared hourly averages of the one minute, ten minute and one hour averages of σ_θ with hourly averages of 10/L. The results are shown in Figure 8.

For unstable conditions somewhat better results were obtained when σ_θ versus ln(-10/L) was plotted and this is shown in Figure 9. For both figures the solid lines are linear regression fits to the data. The open circles in Figure 9 are the averages for all data in the bins $-10/L < 0.1$, $0.1 \leq -10/L < 0.2$, $0.2 \leq -10/L < 0.5$, $0.5 \leq -10/L < 1.0$, $1.0 \leq -10/L$. The linear regression results are

Plot	intercept	slope	correlation
σ_θ vs -10/L, unstable	5.4	2.7	0.45
σ_θ vs 10/L, stable	9.7	26	0.47
σ_θ vs ln(-10/L), unstable	9.2	1.9	0.57

The correlations are not good, but they are not surprising when one considers the wide range of conditions encountered and the region in which the measurements were made. We were not dealing with a spatially homgeneous air mass which had a long fetch over the open ocean. As described above, the area has a complex pattern of eddies and channeling of the wind. With the limited data set we have available it is not possible to bin the data into categories which delineate the local flow conditions, which might reduce some of the observed scatter.

The fact that σ_θ shows a better correlation with ln(-10/L) than with -10/L is rather peculiar, and, in fact, we include Figure 9 only because it better shows that σ_θ is correlated with the Monin-Obukhov length. It would be unreasonable to use a logarithmic dependence on stability, unless

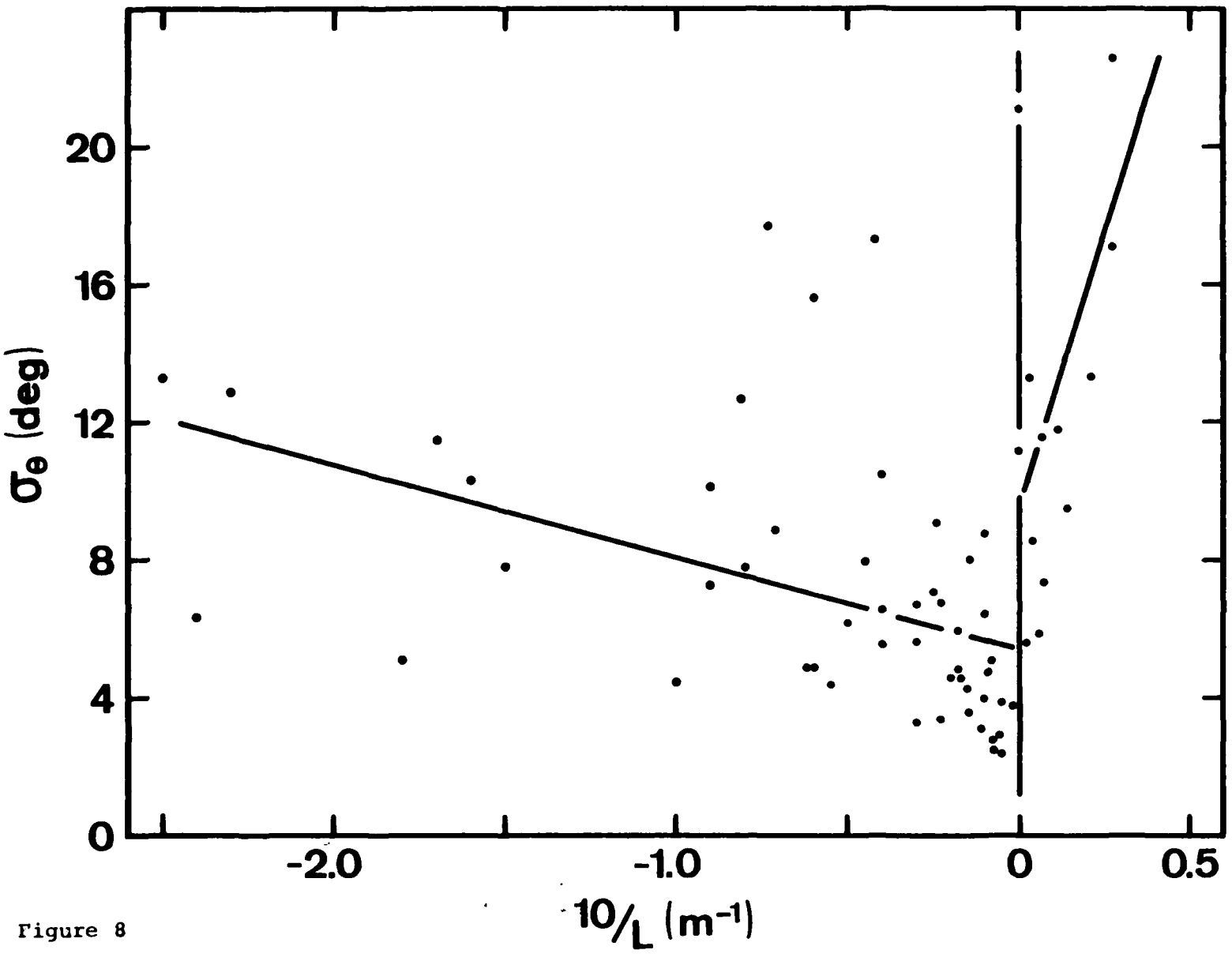

Figure 8

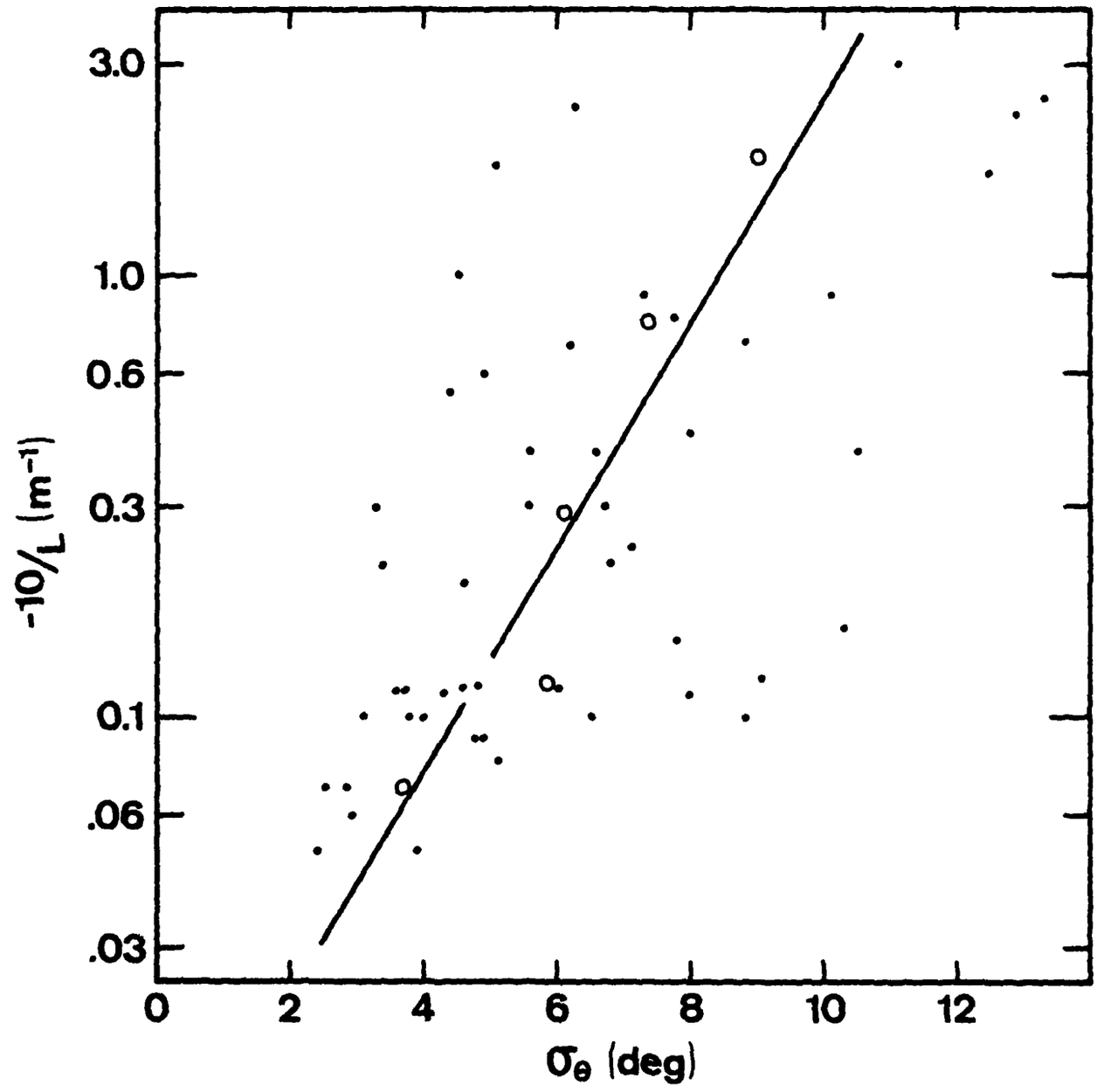

Figure 9

the functions were truncated, since σ_θ would become negative as neutrality is approached.

We have used the above results to determine average relations for σ_θ as a function of 10/L. They are (σ_θ in degrees, L in meters):

stable conditions

$$\sigma_\theta = 12 \qquad (10/L > 0)$$

unstable conditions

$$\sigma_\theta = 5.4 + 2.7(-10/L) \qquad (10/L < 0)$$

or

$$\sigma_\theta = 10.2 + 2.4 \ln(-10/L) \qquad (10/L < -0.05)$$

$$= 3.0 \qquad (-0.05 \leq 10/L < 0)$$

This combination of relations is rather peculiar since they do not agree at 10/L = 0. The linear regression fit to 10/L does not appear to do a good job near neutrality for unstable conditions and is probably meaningless for the small data set for stable conditions data set. The truncated logarithmic fit, and the constant value for stable conditions, best approximate the data we have obtained. Note in Figure 9 that the open circles, which are the average values for the ln(-10/L) bins listed above, are fairly well approximated by the linear regression fit (solid line). One important note must be made: when using Equations 8 and 10 the calculated values of σ_θ can be in error by as much as a factor of ten and errors of a factor of two will be common.

We have attempted to reduce the scatter in the results by plotting σ_θ versus wind direction and 10/L to see if the

local air mass trajectory had an effect. The results are shown in Figure 10, where different symbols are used for four σ_θ bins. The results are not helpful; wind direction does not appear to play an important role.

The most striking aspect of these results is the large σ_θ for slightly stable conditions. Previous experiments, over both land and water, have shown a continuous increase of σ_θ (or σ_y) as atmospheric stability goes from stable to unstable [6,7,8]. We believe the results of this study are location specific. Stable conditions over California coastal waters are unusual, and normally associated with offshore flow or where the air mass has not equilibrated after being transported across a change in sea-surface temperature. In the Ventura area, local eddies or flow over the channel islands could produce a stable surface layer. In both cases, variations in the wind direction could be large due to orographic effects. Such variations would presist over long distances due to the stability of the atmosphere. Thus, the stable results reported here for σ_θ should not be thought to apply to stable onshore flow in open coastal areas.

C. Overwater Modified Pasquill

We have determined one-hour averaged values of the modified classes from the measurements made on the RV/Acania, using the method described in Section V. The measured values of σ_θ and the modified classes for these time periods are shown in Figure 11. Even though there are 48 hours of data, there is insufficient data to yield a good σ_θ versus class

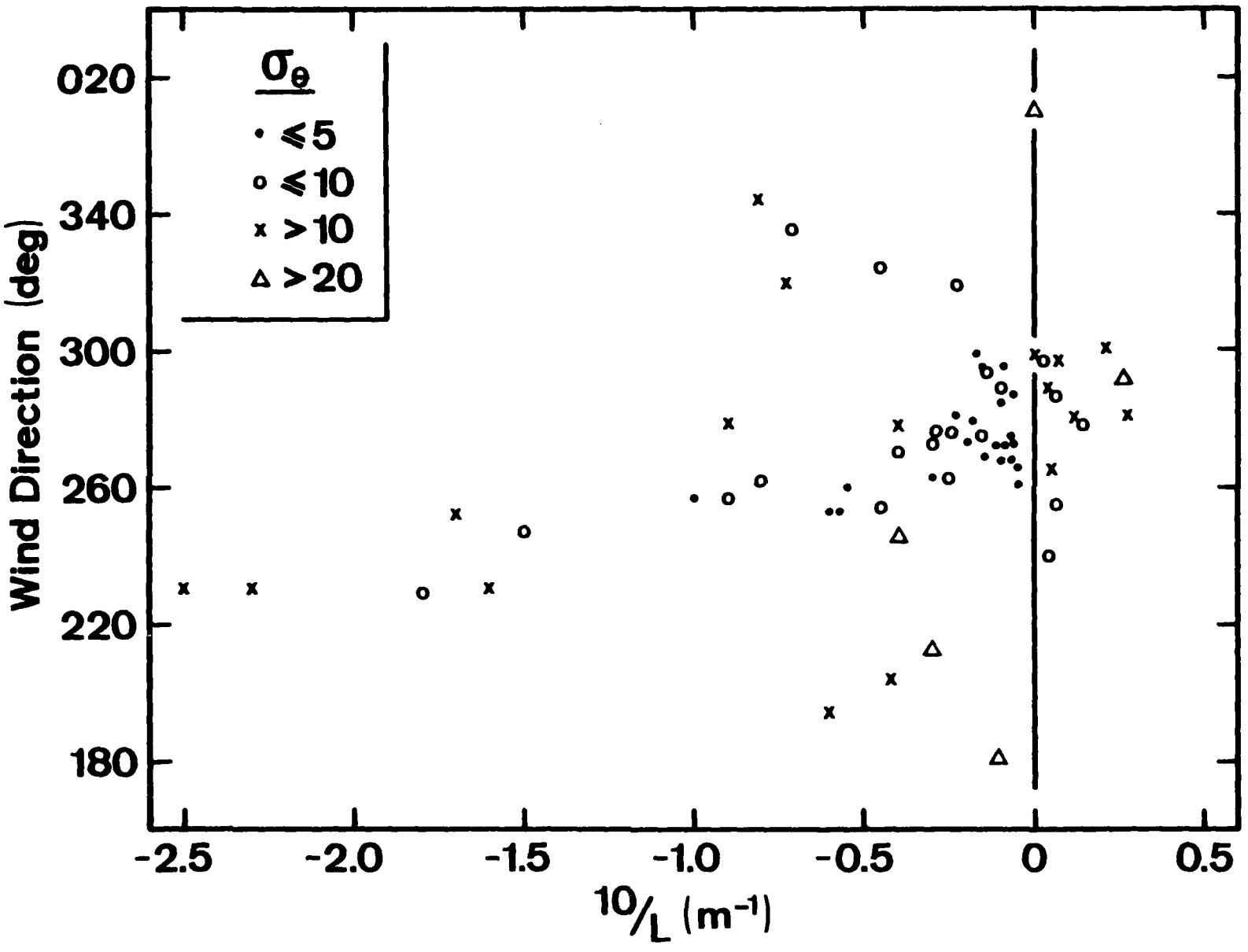
σθ
• ≤5
o ≤10
x >10
Δ >20
Wind Direction (deg)
020
340
300
260
220
180
-2.5
-2.0
-1.5
-1.0
-0.5
0
0.5
10/L (m⁻¹)

Figure 10

relationship because so much of the data are near neutral. We cannot verify that the classes should be divided into subclasses, though it does appear to be valid for class D. The results suggest the following relation to obtain the classes from σ_θ, or vice-versa:

Pasquill Class	σ_θ (deg)
B	10 - 14
C	6 - 10
D (unstable)	2 - 6
D (stable)	7 - 14

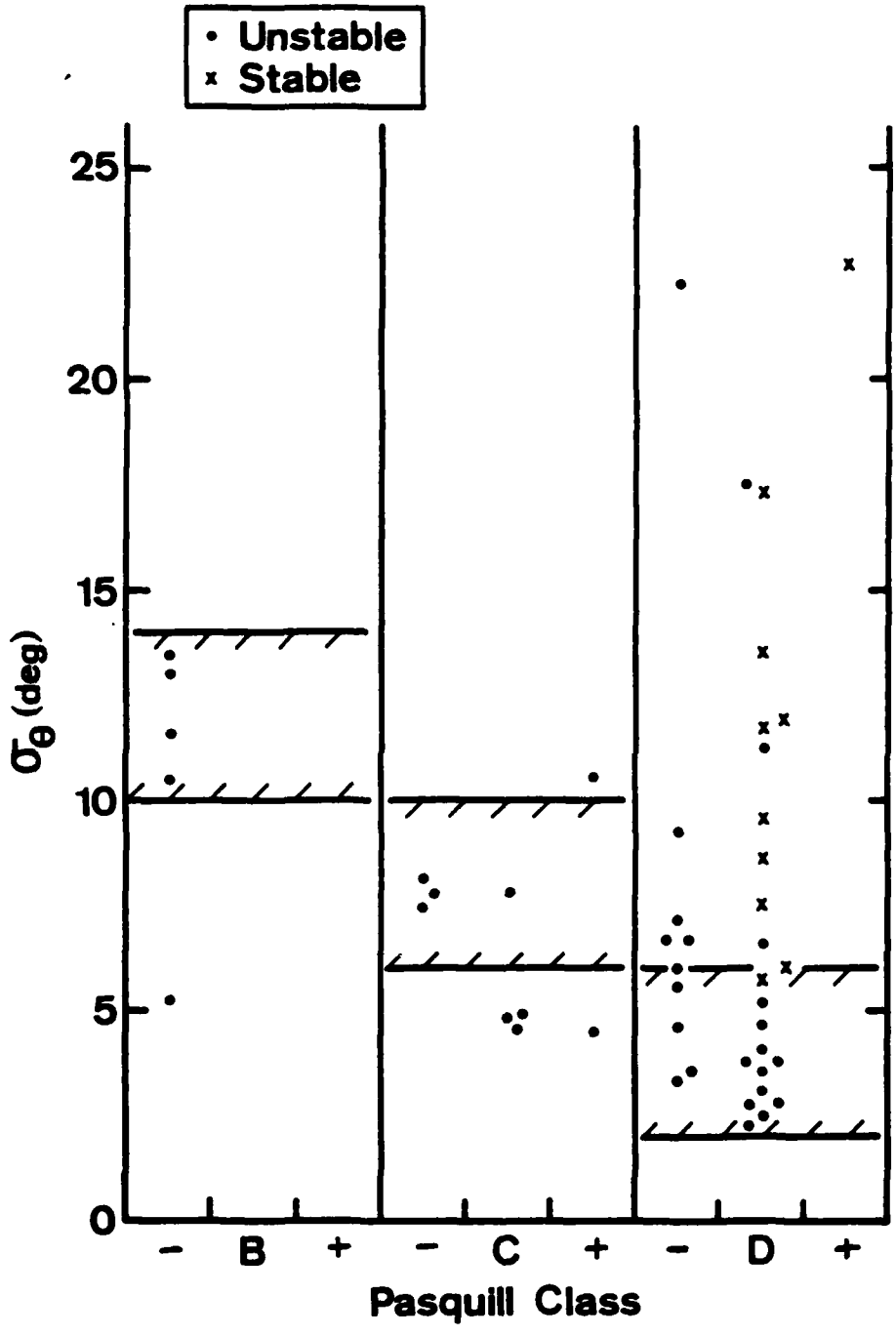
• Unstable
x Stable
25
20
15
10
5
0
σ_θ (deg)
- B +
- C +
- D +
Pasquill Class

Figure 11

APPENDIX A

Determination of Stability and Scaling Parameters

We develop here the method used to determine stability from measured mean meteorological parameters. The method also yields the surface layer scaling parameters, which are directly related to the fluxes. We also show how the convective mixing velocity can be determined. This velocity can be used to determine the rate at which pollutants are mixed through the full boundary layer.

In what follows we use the notation:

T	temperature (K)
Z	height (m)
U	mean wind speed (m/sec)
q	water vapor mixing ratio (g/kg)
$\theta = T + .0098Z$	potential temperature
$\theta_V = \theta + .61Tq$	virtual potential temperature
g	acceleration due to gravity
k	von Karman's constant (0.35)
U_*	friction velocity (scaling velocity)
q_*	mixing ratio scaling parameter
T_*	scaling temperature
w_*	convective mixing velocity
Z_o	roughness length
L	Monin-Obukhov length

z_i	inversion height
X	atmospheric parameter (T, q or U)
α_X	turbulent diffusivity ratio ($\alpha_U = 1$)
X	drag coefficient
ξ	Z/L
$\phi(\xi)$	gradient stability function
$\psi(\xi)$	profile stability function

We describe the stability with the Monin-Obukhov length

$$L = \frac{T\, U_*^2}{kg\, \Theta_{v*}} \quad . \tag{A-1}$$

The scaling parameters are related to the gradients by

$$\frac{dX}{dZ} = \frac{X_*}{\alpha_X kZ}\, \phi_X(\xi) . \tag{A-2}$$

Current best evidence shows that transport of the scalars, heat and water vapor, obey the same relationship to their gradients. Thus, $\phi_T = \phi_q$ and $\alpha_T = \alpha_Q = 1.35$. The stability correction functions are:

$$\phi_T(\xi) = (1 - 9\xi)^{-1/2} \qquad \xi < 0 \qquad \phi_u(\xi) = (1 - 15\xi)^{-1/4}$$

$$= (1 + 6.4\ ) \qquad \xi > 0 \qquad = (1 + 4.7\xi) \tag{A-3}$$

Bulk Method

To obtain the stability, the scaling wind speed and temperature are needed for use in Equation A1. They are obtained from bulk measurements using an integrated form of Equation A2. We integrate Equation A2 from the surface to a reference height Z, usually 10m.

$$X_Z - X_S = \frac{X_*}{\alpha k}\int_o^Z \frac{\phi_X(\xi)}{Z}\,dZ \qquad (A\text{-}4)$$

$$= \frac{X_*}{\alpha k}\left[\ell n\,\frac{Z}{Z_{oX}} - \psi_X(\xi)\right],$$

where X_S is the surface value. We have dropped the subscript on α for convenience.

For analysis of data, it is most convenient to solve Equation A4 for X_* and rewrite in terms of the drag coefficient. The neutral stability drag coefficient is given by

$$\frac{k}{X_N} = \frac{\alpha}{\ell n\, Z/Z_{oX}} \qquad (A\text{-}5)$$

and corrected for stability by

$$\frac{k}{X} = \frac{k}{N_X}[1 - \psi_X(\xi)C_{NX}^{1/2}/\alpha k]^{-1} \qquad (A\text{-}6)$$

Thus, the scaling parameter is given by

$$x_* = C_X^{1/2}(x_Z - x_s) \tag{A-7}$$

As was stated above, the key to the analysis is obtaining the stability. From Equation 1 we write ξ as

$$\xi = \frac{k g Z}{T} \frac{\theta + 0.61 \times 10^{-4} T_q^*}{U_*^2}. \tag{A-8}$$

For the humidity correction term, we use T = 15°C and approximate 0.61 T ≈ 0.18 (q in gm/kg). Rewriting in drag coefficient form gives, for neutral stability,

$$\xi_o = \frac{k g Z}{T} \frac{C_{TN}^{1/2}}{C_{UN}} \frac{(T - T_s) + 0.18 (q - q_s)}{U^2}. \tag{A-9}$$

We assume zero wind speed at the surface. Using Equations A6, A8, and A9 gives

$$\xi = \xi_o \frac{[1 - \psi_u(\xi) C_{UN}^{1/2}/k]^2}{1 - \psi_T(\xi) C_{TN}/\alpha_k} \tag{A-10}$$

Obviously, in order to determine ξ the stability functions must be known and they are determined from ξ. Thus, an iterative procedure must be used. The steps are as follows:

1. Calculate q and q_S from the measured T_S, T, and dew point temperature for Z = 10 m and assuming 100% humidity at the surface.

2. Use $C_{TN} = 1.3 \times 10^{-3}$ and C_{UN} from the table below and the measurements to obtain ξ_o.
3. Calculate ψ_U and ψ_T.
4. Calculate ξ from Equation A10.
5. Iterate steps 3 and 4 until the desired accuracy is obtained, giving ξ.
6. L has been determined and U_*, T_*, and q_* are obtained directly from Equation A7.

For Z = 10 m the wind drag coefficient is found from [5]

U (m/sec)	$C_{UN} \times 10^3$
0.3 - 2.2	$1.08\ U^{-1.5}$
2.2 - 5.0	$0.77 + 0.086U$
5 - 8	$0.87 + 0.067U$
8 - 25	$1.2 + 0.025U$

The profile stability functions are

$$\psi_T(\xi < 0) = 2\,\ell n\left(\frac{1+x}{2}\right) \qquad \text{for } x = (1 - 9\xi)^{1/2}$$

$$\psi_T(\xi > 0) = -6.5\xi \qquad \text{(A-11)}$$

$$\psi_U(\xi < 0) = 2\,\ell n\left(\frac{1+x}{2}\right) + \ell n\left(\frac{1+x^2}{2}\right) - 2\tan^{-1}x + \frac{\pi}{2}$$

$$\text{for } x = (1 - 15\xi)^{1/4} \qquad \text{(A-12)}$$

$$\psi_U(\xi > 0) = -4.7\xi$$

Surface Layer Fluxes

The scaling parameters described above apply to, and specify the state of the surface layer. The surface layer momentum, heat, and water vapor fluxes can be determined from scaling parameters by

$$F_m = \rho U_*^2$$
$$F_h = \rho C_p U_* \Theta_* \qquad \text{(A-13)}$$
$$F_q = \rho U_* Q_*$$

The F_h in Equation A13 is the sensible heat flux. The depth over which the surface scaling applies is approximately $|L|$.

Boundary Layer Scaling

Above the surface layer (ignoring the transition region to the well mixed layer), surface scaling no longer applies and new scaling length, velocity, and temperature are needed. These are:[9]

$$w_* = [(g/T)\, Q_o\, z_i]^{1/3} \qquad \text{(A-14)}$$
$$H_* = Q_o / w_*$$

We assume that the boundary layer depth is defined by the inversion height, z_i. Q_o is the surface virtual heat flux.

w_* is the scaling velocity in the well mixed layer, and we assume that this velocity is directly related to the boundary layer convective mixing velocity. Previous SF_6 tracer experiments performed by California Institute of Technology in

cooperation with NPS have shown that w_* computed by the above method closely predicts the tracer experiment results. Laboratory experiments [10] have also shown that the vertical transport of particulate matter is given by w_*.

Equation A-14 for w_* is not correct for the cloud topped boundary layer. In that case the presence of the cloud modifies the heat flux due to release of latent heat upon condensation and absorption and emission of radiation. The term Q_o in Equation A-14 must be replaced with 2.5 $\langle Q \rangle$, the average heat flux in the boundary layer. Use of the equation as it stands will typically lead to underestimates of about 30% (it is this small due to the one-third power dependence of w_* on Q).

APPENDIX B

Shipboard Meteorological Equipment and Calibration Procedures

The RV/Acania has two meteorological stations at heights of 7.0 and 20.5 meters above mean sea level and a wide range of auxiliary instrumentation. Sensors are mounted on masts in foreward locations so that ship disturbance of the airflow has as little influence as possible. We will not describe all of the shipboard equipment, only that which was used to gather the data for this study. A complete description appears elsewhere[11].

The meteorological stations have equipment to measure the following parameters:

relative wind speed

relative wind direction

air temperature

dew point

Wind direction was measured only at the top level. The true wind speed and direction were calculated from the relative wind speed and direction and the ship's speed and heading. Auxiliary measurements which were made included:

sea surface temperature

inversion height

ship roll

ship heading

Individual Instrumentation

Wind speed and direction: Meteorology Research, Inc., 1022 sensors with 1001 transmuter. The wind direction sensor has dual potentiometers; the transmuter has automatic switching, giving a 0-540° continuous readout. The wind speed sensors are cups with a 0.25 m/sec threshold, 60 m/sec maximum speed, and 1% accuracy.

Dew Point: General Eastern, 1200AP, with 1211P sensor. The system measures the dew point by the cooled mirror technique. The change in the reflectivity of a cooled mirror upon condensation is detected optically. The optical detector is in a servo circuit which controls the mirror temperature, holding it at the dew point. A platinum resistor, bonded to the mirror, is the temperature detector. The sensor is mounted in an aspirated radiation shield suppled by the manufacturer. The system has a range of approximately 70°C below ambient temperature, which is governed by the capacity of the thermoelectric cooler. Operating temperature limits are 100°C to -59°C. Manufacturer stated accuracy is $\pm$ 0.22°C.

The platimum thermometer comes equipped with a three wire hook up for the readout that is supplied with the instrument. The readout converts sensor resistance (three-wire) to a voltage proportional to temperature. Because of drifts in the voltage conversion circuitry, we read the sensor resistance with a computer controlled 4-wire Ohmeter and convert to temperature in computer software. Converting the sensor to a 4-wire system has eliminated lead resistance influence.

Air temperature: Rosemount, 100 Ohm platinum resistors, 4-wire configuration. The resistance is measured with the same computer controlled meter used for the dewpoint measurements. The resistor is mounted in a 1/4 in stainless steel tube. This tube fits loosely in a 3/8 inch tube topped by a small metal enclosure. The enclosure has an environmentally tight screw cap so it may be opened for access to the resistor leads. The outer tube and housing are enclosed in an R.M. Young, Gill aspirator for radiation shielding. The aspirator consists of a silvered glass dewar which is isolated from the heat of the aspiration motor by a long tube. To improve the performance of the aspirator we have mounted a silvered mylar radiation shield at the inlet. This has been found to be especially necessary on shipboard where some sensors are over the water and some over the warm deck of the ship.

In order to eliminate contact e.m.f. problems the 4 wires leads are continuous all the way from the resistor to the Ohmeter. Solder connections are made in the aspirator housing. All solder points are at the same temperature so that thermal e.m.f. is not a factor. The accuracy of the system is $\pm$0.2°C, the uncertainty being due to imperfect aspiration. In order to achieve this accuracy with the 100 Ohm platinum resistor the Ohmeter must have 5 significant figure accuracy.

Sea-Surface Temperature : The sensor is a 100 Ohm platinum resistor identical to that used for air temperature. The sensor is enclosed in a long streamlined float that can be towed at normal ship speed or will remain near the surface when the ship

is stopped. The float is a 12 ft long, 3/4 inch internal diameter, tygon tubing. One end of the tubing is sealed with a brass plug and the sensor is mounted with good thermal contact in this plug. The plug extends 1 inch beyond the end of the tubing so that it makes good thermal contact with the water. The other end, through which the lead passes, is sealed by silicone cement. The sensor is suspended from the side of the ship on a guyed pole so that it is outside the ship's influence. The sensor samples approximately the top 12 inches of the water due to its bobbing with ship motion Accuracy is $\pm$ 0.1°C.

Inversion Height: Aerovironment 300, Acoustic Radar with 100 Watt driver. The device has a range of 100 to 1000 m, but it is difficult to discern an inversion above 700 m. Shipboard noise limits the useful range to about 500 m when the ship is underway. The enclosure used for the antenna is a pentagon with sides 4 ft wide and 8 ft high. For shipboard, the base of the enclosure must be soundproofed. The recently available toothed enclosure extensions, Thenadners, also reduce the noise considerably. The enclosure is normally located near the stern of the ship to reduce wind noise, and in a location where stack noise is minimal.

Ship Heading: On the RV/Acania a Librascope 7070 analog to digital converter has been connected to the gyroscope used for navigation. The converter is a mechanical device that senses the readout angular orientation. A buffer interfaces the output of the converter to a 16 bit interface to the computer.

Ship Roll and Roll Rate: A mechanical pendulum geared to a potentiometer placed on, and pivoting about, the roll axis of the ship, provides an analog signal proportional to the ship's roll angle. A simple RC network is used to differentiate this signal to yield an output related to roll rate. Errors introduced by vertical and lateral accelerations of the ship are minimized by placing the pendulum on the roll axis and midway along the length of the ship.

Data Acquisition Equipment

Three basic methods of data acquisition and shipboard analysis are used: 1) Computer controlled acquisition of all signals, 2) Analog tape recording and strip charts, and 3) Spectral analysis.

Spectral Analysis: Nicolet Scientific Corp., 440B Spectrum analyzer. We have found that spectral analysis is a necessity on shipboard, particularly to monitor fluctuation signals. A ship is an electrically noisy environment, and the noise is not constant. Spectral analysis can help solve noise problems. Frequent monitoring of signals to verify the quality of the data is advisable.

Analog recording: Honeywell 5600E tape recorder. This unit has 14 analog channels and automatic speed control. We have built a selector so that all 14 input or output channels can be monitored on a oscilloscope and by spectral analysis. The recorder is a back up device, all analog signals being recorded in case there is a failure in any other portion of the data acquisition system.

Strip chart recordings are made of the relative wind direction, and any three other parameters, as desired. The strip chart allows post-experiment analysis of the data to be done to pick out times when external influence (such as RFI) could invalidate the data. The strip charts allow these events to be detected (recognizing that qualified personnel may not be available for continuous 24-hour monitoring).

Computer controlled acquisition: Hewlett Packard (HP) 9825 or 9835 desktop computer and HP 3052A data acquisition system. The data acquisition system includes a 59309A digital clock, 3455A digital voltmeter, and 3495A scanner. Data output is on the computer internal tape and a 9871A or a 2631 printer.

The scanner has 40 channels of low thermal emf relays with a switching time of less than 10 msec and a contact differential emf of less than 2 μVolt. The relays are three terminal, accommodating a hi, lo, and ground or guard. This is desirable since the guards for the various signal channels can be kept independent, eliminating ground loops.

The voltmeter has six significant figures resolution, which is needed for the platinum resistance thermometer measurements. Accuracy with the high resolution off is 0.001%.

The interface between the computer, data acquisition system, and printer is the HPIB (IEE-488-1975). In addition, the computer is interfaced with the buffer for the LORAN-C navigation and the ship heading indicator by a 16 bit interface. The computer alternately operates the scanner, interrogates the voltmeter, and

interrogates the buffer. All scanner channels are activated and the data acquired between individual readings of the heading.

Normal shipboard procedure is to produce half-hour averages of all signals. The exact number of samples of each channel depends on the program being used, e.g. some programs do many more calculations and intermediate averages. The number of samples ranges from 800 to 1500. The computation plus print time uses one to two minutes of each half-hour period. During the half-hour cycle all signals are acquired, averaged, computations made, and all averaged voltages and computed parameters are stored on the tape and printed out. Included in the storage and printout are all system calibration parameters so that all calculations can be redone later, if needed.

Calibration Procedures

The results of the laboratory calibrations of meteorological sensors for use in field measurements can be misleading. For example, we can calibrate the platinum resistance temperature sensors to $\pm$ 0.001°C, or can calibrate them with the leads used in the field to $\pm$ 0.01°C. This calibration is repeatable and represents the basic capabilities of the calibration facility. When these sensors are used in the field, with the required aspiration, recognizing that at times the aspirator will be shaded and at times in direct sunlight, measurement accuracy of $\pm$ 0.1°C is doing well. Measuring wind speed is another problem because of ship influence. No matter how accurately the cups are calibrated using them on, or near, the RV/Acania reduces the accuracy to $\pm$ 0.5 m/sec. The results on larger ships are worse. The attainable accuracies in the field are sufficient for this work,

especially when one considers the use of the results. Meteorological parameters measured at a point are being used to predict plume behavior over a spatially large region, near the coast, where spatial inhomogeneities are great. Great accuracy is not required but, of course, the sensors should be moderately well calibrated so that systematic errors are not introduced. As will be seen in the following description of calibration procedures, we are well within that goal.

Air, Sea and Dewpoint Temperatures: All temperature sensors are calibrated together in an insulated chamber. The air and sea temperature probes and a HP2801A quartz thermometer standard are mounted in an aluminum cylinder which effectively eliminates the temperature differences between these sensors. The differences are less than 0.01°C. The dewpoint thermometers cannot be mounted in the same block because they are permanently mounted to the mirror in the sensor. In the chamber we use for calibration, these sensors can be as much as 0.1°C away from the cylinder temperature. The temperature measured by a sensor is found from its resistance by inverting the standard equation

$$R = R_o(1 + \alpha T),$$

where T is in °C, R_o the resistance at the ice point, and α is the temperature coefficient. For the air temperature sensors $\alpha = 0.003921$; for the dewpoint sensors $\alpha = 0.003895$. The calibration procedure is to determine the values of R_o for each sensor from the known temperature and the measured resistances. This is done at several temperatures to eliminate errors which can be introduced by temperature inhomogeneities in the chamber.

Calibration accuracy is ± 0.01°C for the air and sea surface temperature sensors and ± 0.1°C for the dew point sensors.

Wind Speed: Calibrations are performed in one of the NPS wind tunnels using a calibrated hot wire sensor as the standard. We do not attempt to perform the calibration to an accuracy any greater than ± 0.5 m/sec. We have not found any errors or differences between sensors within 0.5 m/sec. Salt loading of the bearings on a sensor can cause it to be outside of this range. This is easily detected long before the calibration is affected by observing the decay rate of the shaft rotation when no cup is in place. Affected sensors are never used.

Inversion Height: The acoustic sounder records are calibrated with radiosondes every 12 hours during most shipboard operations. It is misleading, however, to consider this to be a good calibration of the sounder, it is only semi-quantitative. The acoustic return which the sounder senses comes from reflection from small scale temperature inhomogeneities. The inhomogeneities are caused by a combination of the temperature gradient and mechanical turbulence at the inversion. The return, thus, is not necessarily from the height where the temperature break occurs, which is the inversion height deterined from the radiosonde. Normally, radiosonde and sounder determinations of boundary layer depth agree to within 40m.

References

1. "Offshore Transport and Diffusion in the Los Angeles Bight - I, NPS Data Summary", G.E. Schacher, K.L. Davidson, C.A. Leonard, D.E. Spiel, and C.W. Fairall, Naval Postgraduate School Report NPS-61-81-004, second experiment report NPS-61-81-025 (1981).
"Data Submission for Offshore Tracer Study in Ventura County", Aerovironment, Inc. reports DO81-008, DO80-056, DP80-056 (1981).

2. The descriptions of the local meteorology are exerpted from the following Pacific Missile Range publications.
   a. "Climatic Handbook for Point Mugu and San Nicolas Island, Part I, Surface Data" Robert deViolini, PMR-TP-74-1 (1974).
   b. "Point Mugu Forecasters Handbook" PMR-TP-72-1 (1972).
   c. "Diurnal Wind Behavior at Point Mugu as a Funnction of Wind Direction and Speed at Vandenberg/Point Arguello/ Santa Maria" J. Rosenthal, Atmos. Sci. Tech. Note No.25 (1970).

3. October 1980 revision of Environmental Protection Agency "Guideline on Air Quality Models".

4. Golder, P., Bound. Layer Meteor. 3, 47 (1958).

5. Kondo, J., Bound. Layer Meteor. 9,91 (1975).

6. "A Comparison of Estimation Procedures for Over-Water Plume Dispersion", R.P. Hosker, Jr., Proceedings of the Symposium on Atmospheric Diffusion and Air Pollution, P. 281 (1974), Amer. Meteorological Soc. publication.

7. "A Research Program on Atmospheric Diffusion from an Oceanic Site, G.S. Raynor, P. Michael, R.M. Brown, and S. SethuRaman, Proceedings of the Symposium on Atmospheric Diffusion and Air Pollution, p. 289 (1974), Amer. Meteorological Soc. publication.

8. Slade, D.H., Nuclear Safety 7, 225 (1966).

9. Kaimal, J.C., J.C. Wyngaard, D.H. Haugen, D.R. Cotè, and Y. Izumi, J. Atmos. Sci. 33, 2152 (1976).

10. Willis, G.E. and J.W. Deardorf, J. Atmos. Sci. 31, 1449 (1974).

11. "Naval Postgraduate School Shipboard and Aircraft Meteorological Equipment", G.E. Schacher, K.L. Davidson, D.E. Spiel, and C.W. Fairall, Naval Postgraduate School Report, NPS-61-80-017PR(1980).

DISTRIBUTION LIST

		No. of Copies
1.	Defense Documentation Center Cameron Station Alexandria, Virginia 22314	2
2.	Library, Code 0142 Naval Postgraduate School Monterey, California 93940	2
3.	Dean of Research, Code 012 Naval Postgraduate School Monterey, California 93940	1
4.	Dr. C.W. Fairall BDM Corporation, 1340 Munras St. Monterey, California 93940	2
5.	Mr. Don Spiel BDM Corporation, 1340 Munras St. Monterey, California 93940	2
6.	Professor J. Dyer, Code 61Dy Naval Postgraduate School Monterey, California 93940	1
7.	Dr. Fred Shair 208-41 California Institute of Technology Pasadena, CA 91125	1
8.	Assoc. Professor K.L. Davidson, Code 63Ds Naval Postgraduate School Monterey, California 93940	2
9.	Professor G.E. Schacher, Code 61Sq Naval Postgraduate School Monterey, California 93940	10
10.	Dr. Warren Johnson SRI International 333 Ravenswood Ave. Menlo Park, CA 94025	1
11.	Mr. Robert Harrison Western Oil and Gas Assoc. 727 W. 7th St. Los Angeles, CA 90017	1
12.	Mr. Charles Bennett California Air Resources Board 1709 11th St. Sacramento, CA 95814	1

13. Mr. E.P. Crockett — 1
American Petroleum Institute
2101 L Street N.W.
Washington, D.C. 20037

14. Mr. Stephen S. Wise — 1
Mobile Research and Development Co.
Paulsboro, NJ 08066

15. Professor R.J. Renard, Code 63Rd — 1
Naval Postgraduate School
Monterey, CA 93940

16. Mr. Dick Wilhelmsen — 15
Room 200 OCS Division
Bureau of Land Management
1340 West 6th Street
Los Angeles, CA 90017

17. Mr. David Wilbur — 2
Aerovironment, Inc.
145 North Vista Avenue
Pasadena, CA 91107

18. Mr. Tom Rapolt — 1
Energy Resources Co., Inc.
3344 N. Torrey Pines Ct.
La Jolla, CA 92037

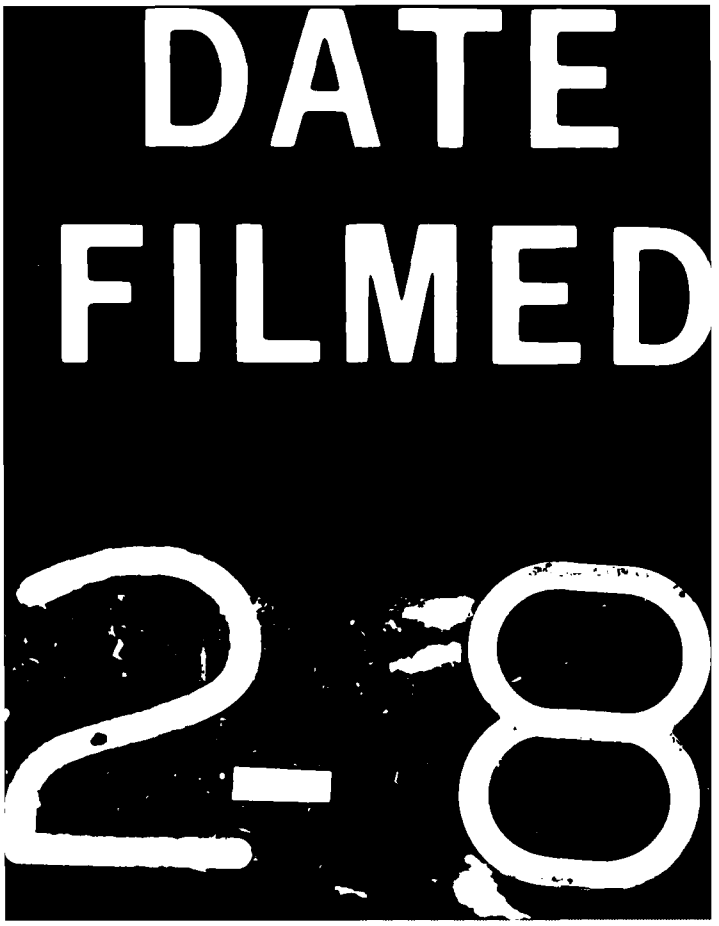
DATE
FILMED
2-8